diagnosed based on the criteria of the international JMML Working Group. Leukemia. 2002;16:645–9.
13. Yoshimi A, Bader P, Matthes-Martin S, Stary J, Sedlacek P, Duffner U, et al. Donor leukocyte infusion after hematopoietic stem cell transplantation in patients with juvenile myelomonocytic leukemia. Leukemia. 2005;19:971–7.
14. Yoshimi A, Mohamed M, Bierings M, Urban C, Korthof E, Zecca M, et al. Second allogeneic hematopoietic stem cell transplantation (HSCT) for patients with juvenile myelomonocytic leukemia. Leukemia. 2007;21:556–60.
15. Inagaki J, Fukano R, Nishikawa T, Nakashima K, Sawa D, Ito N, et al. Outcomes of immunological investigations for mixed chimerism following allogeneic stem cell transplantation in children with juvenile myelomonocytic leukemia. Pediatr Blood Cancer. 2012;60:116–20.
16. Yoshimi A, Niemeyer CM, Bohmer V, Duffner U, Strahm B, Kreyenberg H, et al. Chimaerism analyses and subsequent immunological intervention after stem cell transplantation in patients with juvenile myelomonocytic leukemia. Br J Haematol. 2005;129:542–9.

Biol Blood Marrow Transplant 21 (2015) 319–325

Biology of Blood and Marrow Transplantation

journal homepage: www.bbmt.org

# Choreito Formula for BK Virus–associated Hemorrhagic Cystitis after Allogeneic Hematopoietic Stem Cell Transplantation

Nozomu Kawashima, Yoshinori Ito, Yuko Sekiya, Atsushi Narita, Yusuke Okuno, Hideki Muramatsu, Masahiro Irie, Asahito Hama, Yoshiyuki Takahashi, Seiji Kojima*

*Department of Pediatrics, Nagoya University Graduate School of Medicine, Nagoya, Japan*

*Article history:*
Received 28 August 2014
Accepted 21 October 2014

*Key Words:*
BK virus
Hemorrhagic cystitis
Pediatric
Choreito
Kampo medicine

A B S T R A C T

Therapy for BK virus (BKV)–associated hemorrhagic cystitis (BKV-HC) is limited after hematopoietic stem cell transplantation (HSCT). We examined whether choreito, a formula from Japanese traditional Kampo medicine, is effective for treating BKV-HC. Among children who underwent allogeneic HSCT between October 2006 and March 2014, 14 were diagnosed with BKV-HC (median, 36 days; range, 14 to 330 days) after HSCT, and 6 consecutive children received pharmaceutical-grade choreito extract granules. The hematuria grade before treatment was significantly higher in the choreito group than in the nonchoreito group ($P = .018$). The duration from therapy to complete resolution was significantly shorter in the choreito group (median, 9 days; range, 4 to 17 days) than in the nonchoreito group (median, 17 days; range, 15 to 66 days; $P = .037$). In 11 children with macroscopic hematuria, the duration from treatment to resolution of macroscopic hematuria was significantly shorter in the choreito group than in the nonchoreito group (median, 2 days versus 11 days; $P = .0043$). The BKV load in urine was significantly decreased 1 month after choreito administration. No adverse effects related to choreito administration were observed. Choreito may be a safe and considerably promising therapy for the hemostasis of BKV-HC after HSCT.



## INTRODUCTION

Hemorrhagic cystitis (HC) is a severe complication in patients undergoing hematopoietic stem cell transplantation (HSCT), resulting in significant morbidity, such as nephropathy and renal failure, prolonged hospitalization, and prolonged blood transfusion requirement [1,2]. Effects on mortality have also been reported in children undergoing HSCT [3]. Early-onset HC occurs within 1 week after HSCT and is mostly a symptom of regimen-related toxicity. Late-onset HC usually occurs after engraftment and is associated with viral infections, including those caused by the human polyomavirus BK (BKV), polyomavirus JC, adenovirus (AdV), and cytomegalovirus (CMV) [4]. BKV is the most frequent cause of late-onset HC and affects 5.3% to 21.2% of children undergoing HSCT [5-9]. BKV viruria is detected by real-time quantitative PCR (RT-PCR) in all patients with BKV-HC. A BKV load of more than $10^6$ copies/mL in urine may be associated with a high risk of developing HC after HSCT [5]. However, asymptomatic BK viruria is detected in 50% to 100% of patients after HSCT [5,7,10], implicating that the presence of BKV viruria alone does not explain the pathogenesis of HC. High BKV viremia ($\geq 10^3$ copies/mL) is a better predictor of BKV-HC after HSCT, with a reported specificity of 93% [8]. Children with high BKV viremia ($\geq 10^4$ copies/mL) are at a higher risk of developing severe HC [6].

The standard treatment for BKV-HC has not been established [2]. Supportive therapy is provided to patients with mild BKV-HC, including intravenous hydration, bladder irrigation, and symptomatic relief treatment, such as the use of analgesics. Patients with severe BKV-HC require additional therapy. The current first line BKV-oriented therapy is intravenous cidofovir; however, its efficacy remains controversial [2]. Alternative strategies include intravesical instillation of cidofovir [2,7], hyperbaric oxygen therapy [11], leflunomide, and fluoroquinolone [12]; however, their effect is limited [13]. Invasive intervention such as vascular embolization or cystectomy may be necessary in uncontrollable HC.

Choreito is a formula derived from Japanese traditional Kampo medicine. The indication for choreito in the context of

*Financial disclosure:* See Acknowledgments on page 324.

* Correspondence and reprint requests: Seiji Kojima, MD, PhD, Department of Pediatrics, Nagoya University Graduate School of Medicine, 65 Tsurumai-cho, Showa-ku, Nagoya, Aichi, 466-8550 Japan.
*E-mail address:* kojimas@med.nagoya-u.ac.jp (S. Kojima).

http://dx.doi.org/10.1016/j.bbmt.2014.10.018
1083-8791/

Kampo medicine is "dampness-heat" in the lower abdomen, the characteristic symptoms of which include dysuria, heat in the lower abdomen, and thirst. All these symptoms may be caused by inflammation and blood clots in the bladder. Based on this indication, choreito has been administered to patients with acute simple cystitis and urolithiasis, and its effectiveness has been confirmed [14]. Recently, choreito was successfully used to treat massive gross hematuria with clot retention in the bladder in a child with refractory acute lymphoblastic leukemia [14]. At present, choreito is covered by the national health insurance and is widely used for genitourinary symptoms in Japan.

Symptoms leading to the traditional use of choreito appear to overlap with symptoms associated with BKV-HC; indeed, some children receive choreito for HC. In this study, we retrospectively analyzed BKV-HC in children undergoing HSCT and evaluated the efficacy of choreito treatment.

## PATIENTS AND METHODS

### *Definition*

*HC* was defined as microscopic (blood in urine graded 1+ or more) or macroscopic hematuria combined with dysuria, pollakisuria, urinary urgency, and/or the sensation of residual urine in the absence of bacteria in urine as observed by culture [9]. *BKV-HC* was defined as the association of HC with BKV viruria and/or viremia. HC was graded according to the widely used criteria [15]. Grade I is defined as microscopic hematuria, grade II as macrohematuria, grade III as macroscopic hematuria with clots, and grade IV as macroscopic hematuria with renal or bladder dysfunction. The onset of BKV-HC was defined as the first day when patients presented with urinary symptoms, and *complete resolution* (CR) of HC was defined as blood in urine (− or ± for hemoglobin) and disappearance of dysuria, pollakisuria, urinary urgency, and the sensation of residual urine related to HC.

### *Patient Inclusion Criteria of BKV-HC and Choreito Administration*

Among the children (≤18 years old) who received allogeneic HSCT between October 2006 and March 2014 in Nagoya University Hospital, 14 were diagnosed with BKV-HC and included in the study. Their medical records were retrospectively analyzed. Patient characteristics are listed in Table 1. Intravenous fluids corresponding to 2.5 to 3.0 L/m$^2$/day with forced alkalinized diuresis were administered during conditioning, and patients treated with cyclophosphamide received prophylactic mesna for the prevention of HC. All the patients received acyclovir for herpes prophylaxis and weekly intravenous immunoglobulin for viral prophylaxis. Tacrolimus was intravenously administered for graft-versus-host disease (GVHD) prophylaxis in patients receiving HSCT from an unrelated donor. Cases of engraftment syndrome and GVHD were treated by methylprednisolone, followed by salvage therapies in nonresponding patients. Six children with BKV-HC diagnosed after March 2013 received a pharmaceutical-grade medicine, choreito extract granules (Tsumura & Co., Tokyo, Japan) with a dose of .2 g/kg per os daily in 3 divided doses (maximum, 7.5 g/day). Cidofovir and choreito were administered at the onset of macroscopic hematuria. Because it is not currently approved for clinical use in Japan, cidofovir was administered only to those who provided written informed consent.

### *Quantification of BKV DNA*

Children undergoing HSCT were weekly monitored for plasma CMV, human herpesvirus 6, and Epstein-Barr virus, and those who met the criteria for HC underwent additional viral workup, including analysis for BKV, polyomavirus JC, and AdV. For 2 patients with BKV diagnosed before December 2009, BKV had been detected in urine by qualitative PCR. This qualitative PCR could not detect BKV in patients without HC. After January 2010, viruses were monitored by multiplex RT-PCR for quantification of DNA from BKV, polyomavirus JC, and AdV, as described previously [16]. In April 2010, BKV RT-PCR was used to screen all 30 hospitalized children with various hemato-oncological diseases who had neither HC-related symptoms nor abnormal urinalysis. All patients provided informed consent for viral PCR workup in accordance with the Declaration of Helsinki. This retrospective analysis was approved by the ethics committee of Nagoya University Graduate School of Medicine.

### *Statistical Analysis*

Statistical analysis was performed using the Fisher's exact test for categorical variables and the Mann-Whitney's U test for continuous variables. The Wilcoxon signed-rank test was used for paired samples. Odds ratios with confidence intervals were estimated by the logistic regression. A probability ($P$) value <.05 was considered to indicate statistical significance. All statistical analyses were conducted using JMP Pro 11.0.0 (SAS Institute Inc., Cary, NC).

## RESULTS

### *BKV Screening in Hemato-oncological Patients without Genitourinary Symptoms*

All children with hemato-oncological disorders hospitalized in the same ward were screened for BKV viruria for the purpose of surveillance. BKV viruria was detected in 5 (17%) of 30 hospitalized children with various hemato-oncological diseases who had neither HC-related symptoms nor abnormal urinalysis. The median urine BKV load in children with asymptomatic viruria was $1.3 \times 10^6$ copies/mL (range, $3.5 \times 10^3$ to $2.0 \times 10^9$ copies/mL), which was significantly lower than that in children with BKV-HC (median, $5.4 \times 10^{10}$ copies/mL; range, $8.3 \times 10^7$ to $1.5 \times 10^{11}$ copies/mL; $P = .0021$).

### *Patient Characteristics of Cases with BKV-HC after HSCT*

Table 1 summarizes the patient characteristics of 14 children who underwent HSCT and later developed BKV-HC. In patients 1 and 2, BKV was detected in urine by qualitative

**Table 1**
Patient Demographics of BKV-HC after HSCT

| UPN | Choreito Treatment | Age, yr | Sex | Diagnosis | Clinical Status | Preconditioning Regimen | Stem Cell Source | GVHD Prophylaxis |
|---|---|---|---|---|---|---|---|---|
| 1 | No | 15.3 | M | AA | Non CR | CY + ATG + TBI 5 Gy | UR-BM | FK + sMTX |
| 2 | No | 16.0 | M | AA | Non CR | FLU + CY + Campath + TBI 3 Gy | UR-BM | FK + sMTX |
| 3 | No | 12.3 | M | B-ALL | CR1 | MEL + TBI 12 Gy | UR-BM | FK + sMTX |
| 4 | No | 11.8 | M | CML | CyCR | FLU + MEL + TBI 3 Gy | UR-BM | FK + sMTX |
| 5 | No | 7.1 | F | T-ALL | CR2 | FLU + MEL + ATG + TBI 12 Gy | Haplo | FK + sMTX |
| 6 | No | 5.7 | M | NB | CR1 | FLU + MEL + TBI 2 Gy | UR-CB | FK + sMTX |
| 7 | No | 15.4 | M | CMML | Non CR | FLU + MEL + ATG + TBI 5 Gy | Haplo | FK + sMTX |
| 8 | No | 7.8 | M | B-ALL | CR2 | MEL + ATG + TBI 12 Gy | UR-BM | FK + sMTX |
| 9 | Yes | 14.3 | M | AA | Non CR | FLU + MEL + ATG + TBI 3 Gy | Haplo | FK + sMTX |
| 10 | Yes | 5.4 | M | MDS | Non CR | FLU + MEL + ATG + TBI 5 Gy | Haplo | FK + sMTX |
| 11 | Yes | 10.1 | F | AA | Non CR | FLU + MEL + ATG + TBI 5 Gy | Haplo | FK + sMTX |
| 12 | Yes | 12.2 | F | CMML | Non CR | FLU + MEL + ATG + TBI 5 Gy | Haplo | FK + sMTX |
| 13 | Yes | 6.8 | M | B-ALL | CR2 | MEL + TBI 12 Gy | UR-BM | FK + sMTX |
| 14 | Yes | 7.5 | M | MDS | Non CR | FLU + MEL + ATG + TBI 5 Gy | Haplo | FK + sMTX |

UPN indicates unique patient number; M, male; AA, aplastic anemia; Cy, cyclophosphamide; ATG, antithymocyte globulin; TBI, total body irradiation; UR, unrelated; BM, bone marrow; FK, tacrolimus; sMTX, short course of methotrexate; FLU, fludarabine; Campath, alemtuzumab; ALL, acute lymphoblastic leukemia; MEL, melphalan; CML, chronic myelogenous leukemia; CyCR, cytological complete remission; F, female; Haplo, haploidentical transplant; NB, neuroblastoma; CB, cord blood; CMML, chronic myelomonocytic leukemia; MDS, myelodysplastic syndrome.

PCR; therefore, other agents including preconditioning could have contributed to HC. Six of the 14 children received choreito because of BKV-HC. All patients were older than 5 years (median, 11 years; range, 5.4 to 16 years). Antithymoglobulin or alemtuzumab was administered to 10 of 14 children (71%) as a preconditioning. Notably, all the children received total body irradiation with various doses.

Children were diagnosed with BKV-HC at a median 36 days (range, 14 to 330 days) (Table 2) after HSCT. Six of 14 patients (43%) had grade II to IV acute GVHD, and 11 of 14 (79%) received steroids for treatment of engraftment syndrome and/or acute GVHD before being diagnosed with BKV-HC. Three children with acute GVHD grade III or IV received intensified immunosuppressive treatment for steroid-resistant GVHD; 1 received infliximab and the other 2 received infliximab, basiliximab, and mesenchymal stem cells. All 3 responded well to additional therapy for acute GVHD. Concomitant AdV viruria was detected in 2 of 14 children (14%), and 12 of 14 children (86%) developed CMV and/or Epstein-Barr virus infection after HSCT. AdV titers in the urine were $2.6 \times 10^8$ copies/mL in patient 3 and $1.8 \times 10^8$ copies/mL in patient 7 at the time of diagnosis. CMV viruria was not detected in any of these 14 children when BKV-HC was diagnosed. Six children were receiving gancyclovir and/or foscarnet for CMV reactivation at the time of BKV-HC diagnosis.

### *Treatment for BKV Cystitis with Choreito*

Six of 14 children with BKV-HC diagnosed after October 2013 received choreito (Tables 1 to 3). All 6 fulfilled the Kampo indication for receiving choreito ("lower energizer dampness-heat" in patients 9, 11, 12, 13, and 14, and "heat binding in the lower energizer" in patient 10). Patient characteristics, including age at HSCT, sex, underlying disease, engraftment syndrome, acute GVHD frequency and grade, immunosuppressive treatment, absolute lymphocyte count, antiviral therapy, duration of steroid use before the diagnosis of BKV-HC, and duration from HSCT to the onset of BKV-HC, did not differ significantly between the choreito group and the nonchoreito group (Tables 1 and 2). However, the hematuria grade at the time of diagnosis of BKV-HC was significantly higher in the choreito group than in the nonchoreito group ($P = .018$) (Table 2). Choreito was administered over a median of 5 days after the onset of symptoms related to BKV-HC (range, 2 to 16 days), and this interval was not statistically different from that of other treatments (median, 4 days; range, 1 to 23 days; $P = .43$) (Table 3). The urine BKV load before treatment amounted to a median of $2.6 \times 10^{10}$ copies/mL (range, $1.3 \times 10^9$ to $6.3 \times 10^{10}$ copies/mL) in children receiving choreito, which was not statistically different from that in those not receiving choreito (median, $3.4 \times 10^{10}$ copies/mL; range, $8.3 \times 10^7$ to $1.3 \times 10^{11}$ copies/mL; $P = .67$) (Table 3). Similarly, the BKV load in whole blood before treatment was not statistically different between the choreito and nonchoreito groups ($P = .24$, Table 3).

In all 14 children with BKV-HC, the duration from the start of therapy to CR as defined by disappearance of dysuria, pollakisuria, urinary urgency, and the sensation of residual urine was significantly shorter in the choreito group (median, 9 days; range, 4 to 17 days) than in the nonchoreito group (median, 17 days; range, 15 to 66 days; $P = .037$) (Table 3, Figure 1A): the odds ratio of choreito versus nonchoreito was .63 (95% confidence interval, .22 to .93; $P = .0031$). With regard to 11 children with HC graded ≥ II at the beginning of therapy, the administration of choreito

**Table 2**
Clinical Characteristics of Patients with BKV Cystitis

| UPN | Engraftment Syndrome | Acute GVHD | | ALC at the Diagnosis of BKV-HC ($\times 10^9$/L) | Steroid Use (d before BKV-HC) | Other Immunosuppressants | Onset of BKV-HC (d from SCT) | Hematuria (Grade) | Viruria (Urine log copy/mL) | CMV (Whole Blood log copy/mL) | Viral Infections | Antiviral Therapy at BKV-HC |
|---|---|---|---|---|---|---|---|---|---|---|---|---|
| | | Stage | Grade | | | | | | | | | |
| 1 | + | - | - | 4.7 | 14 | - | 35 | II | BKV | 0.0 | CMV, EBV | GCV |
| 2 | - | skin 3 | II | .3 | 24 | - | 65 | II | BKV | 3.1 | CMV | PFA |
| 3 | + | - | - | .8 | 10 | - | 36 | III | BKV (9.2), AdV (8.4) | 0.0 | CMV | PFA |
| 4 | + | skin 3 | II | 1 | 90 | - | 330 | II | BKV (7.9) | 0.0 | CMV, EBV | PFA |
| 5 | + | skin 2, gut 1 | II | .2 | - | - | 14 | II | BKV (10.8) | 2.6 | CMV | - |
| 6 | - | skin 2, gut 3 | III | 1 | 10 | INX | 45 | I | BKV (10.9) | 0.0 | - | - |
| 7 | - | skin 3, gut 2 | III | .6 | 67 | INX, BSX, MSC | 86 | I | BKV (11.1), AdV (8.3) | 3.0 | CMV, EBV | - |
| 8 | + | - | - | .2 | 2 | - | 27 | II | BKV (10.0) | 3.2 | CMV | - |
| 9 | - | - | - | .2 | - | - | 16 | III | BKV (9.1) | 2.9 | EBV | - |
| 10 | + | skin 2, liver 4, gut 2 | IV | .8 | 12 | INX, BSX, MSC | 25 | III | BKV (9.2) | 0.0 | - | - |
| 11 | + | - | - | 1.8 | 30 | - | 48 | III | BKV (9.5) | 0.0 | CMV, EBV | GCV + PFA |
| 12 | + | - | - | .2 | 45 | - | 67 | III | BKV (10.8) | 2.7 | CMV | GCV |
| 13 | - | - | - | 1.3 | - | - | 21 | III | BKV (10.7) | 0.0 | CMV | - |
| 14 | + | - | - | .5 | 6 | - | 26 | I | BKV (10.7) | 0.0 | EBV | - |

ALC indicates absolute lymphocyte count; SCT, stem cell transplanation; EBV, Epstein-Barr virus; GCV, gancyclovir; PFA, foscarnet; INX, infliximab; BSX, basiliximab; MSC, mesenchymal stem cell transplantation.

**Table 3**
Summary of Treatment for Patients with BKV Cystitis

| UPN | Duration from Onset to Tx, d | Primary Tx for BKV | Hematuria Grade at Tx | Hematuria Grade ≤I (d from Tx) | CR (d from Tx) | Urine BKV Load before Tx (log copy/mL) | Plasma BKV Load before Tx (log copy/mL) | Urine BKV Load 1 mo after Tx (log copy/mL) | Plasma BKV Load 1 mo after Tx (log copy/mL) | Possible Complications |
|---|---|---|---|---|---|---|---|---|---|---|
| 1 | 7 | Cidofovir (5 mg/kg qwk ×2), hydration | II | 11 | 17 | N/A | N/A | N/A | N/A | None |
| 2 | 4 | Bladder irrigation, hydration | II | 16 | 55 | N/A | N/A | N/A | N/A | None |
| 3 | 14 | Cidofovir (1 mg/kg qwk ×2), hydration | III | 28 | 66 | 9.2 | 0.0 | 6.5 | 3.8 | Renal failure |
| 4 | 4 | Hydration | II | 10 | 15 | 7.9 | 0.0 | N/A | N/A | None |
| 5 | 2 | Hydration | II | 5 | 16 | 10.8 | 0.0 | N/A | N/A | None |
| 6 | 1 | Hydration | I | N/A | 15 | 10.9 | 3.0 | 10.5 | 3.6 | None |
| 7 | 1 | Hydration | I | N/A | 15 | 11.1 | 0.0 | N/A | N/A | None |
| 8 | 23 | Hydration | II | 8 | 23 | 10.0 | 0.0 | N/A | N/A | None |
| 9 | 16 | Choreito, cidofovir (1 mg/kg qwk ×11), hydration | III | 4 | 6 | 9.1 | 4.0 | 8.7 | 4.6 | None |
| 10 | 5 | Choreito | III | 2 | 4 | 9.2 | 3.1 | 8.3 | 4.0 | None |
| 11 | 2 | Choreito | III | 2 | 16 | 9.5 | 0.0 | 7.8 | 0.0 | None |
| 12 | 4 | Choreito | III | 3 | 17 | 10.8 | 0.0 | 8.2 | 5.8 | None |
| 13 | 5 | Choreito | III | 2 | 7 | 10.7 | 5.0 | 4.4 | 0.0 | None |
| 14 | 16 | Choreito | I | N/A | 11 | 10.7 | 2.1 | 10.5 | 3.2 | None |

Tx indicates treatment; qwk, every week; N/A, not applicable or available.

significantly shortened the duration from the onset to BKV-HC grade ≤ I (median, 2 days; range, 2 to 4 days) in comparison with that in the nonchoreito group (median, 11 days; range, 5 to 28 days; $P = .0043$) (Table 3, Figure 1B). The duration from start of therapy to CR was also significantly shorter in the choreito group (median, 7 days; range, 4 to 17 days) than in the nonchoreito group (median, 20 days; range, 15 to 66 days; $P = .048$) (Table 3, Figure 1C); here, the odds ratio of choreito versus nonchoreito was .66 (95% confidence interval, .14 to .95; $P = .0058$).

### *Sequential Analysis of BKV Load after Choreito Treatment*

BKV-HC–related symptoms improved significantly earlier in children receiving choreito, and we studied whether these earlier improvements were related to the clearance of BKV. The BKV load in urine and whole blood was monitored after the diagnosis of BKV-HC in children receiving choreito. The urine BKV load generally decreased over time. The median urine BKV load was $1.7 \times 10^8$ copies/mL (range, $2.6 \times 10^4$ to $3.1 \times 10^{10}$ copies/mL) 1 month after BKV-HC diagnosis when all children had achieved CR, and they experienced a statistically significant decrease in BKV load since the time of diagnosis ($P = .031$; Wilcoxon signed-rank test for paired samples) (Table 3, Figure 2A). At the time of CR, only 1 of 6 children had a urine BKV load lower than $1.3 \times 10^6$ copies/mL, which was the median urine BKV load in children with asymptomatic viruria. The BKV load in whole blood appeared stable during the course of BKV-HC, and no significant decrease was observed a month after diagnosis ($P = .44$) (Table 3, Figure 2B).

All 6 children eventually finished taking choreito, and relapse of HC was not observed, except for in 1 patient who experienced relapse twice (patient 9). This patient was diagnosed with idiopathic aplastic anemia and received a bone marrow transplant from an unrelated donor; however, the graft was rejected and he underwent haplo-identical HSCT as the second HSCT. Because he developed chronic GVHD, he was administered prednisolone, which was increased during the exacerbation of chronic GVHD and which may have contributed to the prolonged elevation of the BKV load. Every time the patient had a relapse of BKV-HC, he was administered choreito, and his genitourinary symptoms resolved within a few days (Supplemental Figure 1).

### *Safety and Tolerability of Treatment*

All children were able to take choreito per os. Notably, there were no adverse effects due to choreito intake, and renal function impairment was not observed in children receiving choreito (Table 3). The reported adverse effects of choreito include drug allergy and mild gastric discomfort [14], which were not observed in any of the children. In the nonchoreito group, 1 patient (patient 3) who received cidofovir for BKV infection developed impaired renal function, possibly resulting from renal toxicity of cidofovir and post-renal acute kidney injury due to clot retention.

## DISCUSSION

Unlike its effect in immunocompetent patients, HC is life threatening in immunocompromised patients with hemato-oncological disease, particularly among patients undergoing HSCT [17]. To our knowledge, prospective studies of the treatment for BKV-HC are not available, and there are no standard treatment guidelines for post-HSCT HC. Treatment modalities are limited, particularly in children, partly owing to few reports on children receiving pharmaceutical and

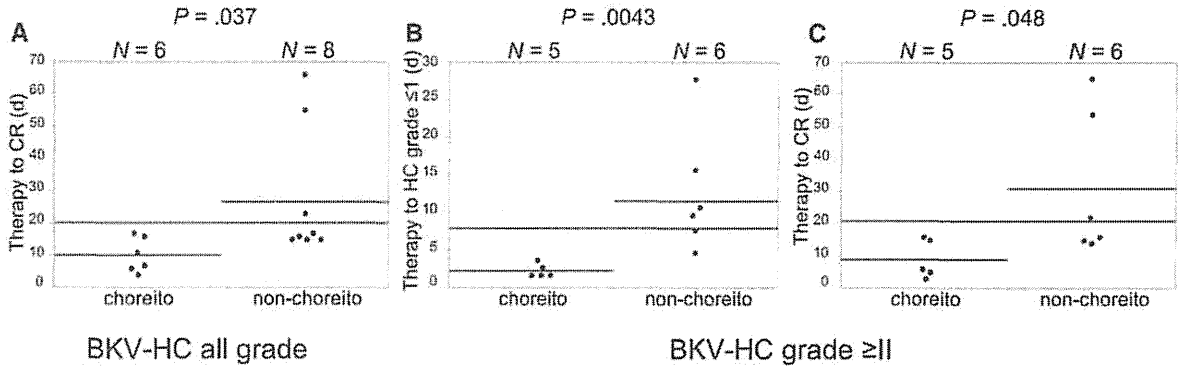


**Figure 1.** Comparison of choreito and nonchoreito treatment for BK virus-associated hemorrhagic cystitis (BKV-HC). The duration from the beginning of therapy to complete resolution (CR), as defined by the absence of dysuria, pollakisuria, urinary urgency, or the sensation of residual urine, was shorter in the choreito group (median, 9 days; range, 4 to 17 days) than in the nonchoreito group (median, 17 days; range, 15 to 66 days; $P = .037$) (A). When comparing children with HC graded ≥ II, the administration of choreito significantly shortened the duration from the onset to BKV-HC grade ≤ I (median, 2 days; range, 2 to 4 days) in comparison with that in the nonchoreito group (median, 11 days; range, 5 to 28 days) (B). The duration from start of therapy to CR was also significantly shorter in the choreito group (median, 7 days; range, 4 to 17 days) than in the nonchoreito group (median, 20 days; range, 15 to 66 days; $P = .048$) (C).

surgical treatments [4,18-20]. Intravenous hydration with forced diuresis is conducted; however, this is supportive treatment only without reliable efficacy.

At present, cidofovir is the only commercially available antiviral agent against BKV, and its efficacy for BKV-HC has been investigated only in retrospective studies [19-21]. In the report from the European Group for Blood and Marrow Transplantation, intravenous or intravesical cidofovir was administered to 62 patients with BKV-HC [21]. Of the 62 patients, 41 (66%) achieved CR and 8 (13%) had partial response after cidofovir treatment; however, no improvement or deterioration was observed in 12 patients (19%). CR is related to clearance of BK viremia in patients with BK viremia detected at the beginning of treatment, and the median time to clearance is 37 days (range, 7 to 102 days). Of 57 patients receiving intravenous cidofovir, 17 (30%) experienced renal toxicity. In a pediatric cohort, 19 children received cidofovir for BKV-HC grade ≥ II [19]. Macroscopic hematuria resolved in 15 (79%) after a median of 22 days (range, 9 to 63 days). In 1 patient, HC progressed to grade IV during cidofovir treatment. Notably, the baseline creatinine level appeared to be elevated after treatment. Another pediatric cohort included 12 children with BKV-HC treated by intravenous and/or intravesical cidofovir [20]. The median duration of symptoms was 25 days (range, 9 to 73 days) and no persistent nephrotoxicity was observed. Compared with cidofovir treatment, children treated with choreito treatment in our study experienced no impairment of renal function; all patients with BKV-HC achieved CR and BKV-HC resolved earlier.

Hyperbaric oxygen therapy is another alternative treatment for BKV-HC [11,22]. A retrospective study included 16 patients with BKV-HC grade ≥ II (5 patients under 19 years of age), 15 (94%) of whom achieved CR after a median of 17 days (range, 4 to 116 days) [11]. In a pediatric cohort of 10 children with BKV-HC grade ≥ II, 9 (90%) achieved CR after a median of 15 days (range, 10 to 37 days), including spontaneous resolution [22]. Hyperbaric oxygen is generally well tolerated; however, it requires a high-cost facility and adverse effects have been reported, including ruptured tympanum.

Other alternative therapies include leflunomide and fluoroquinolone antibiotics [12]; however, experience is limited, even in adults [13]. Few reports of leflunomide use in the setting of HSCT are available and its safety has not been

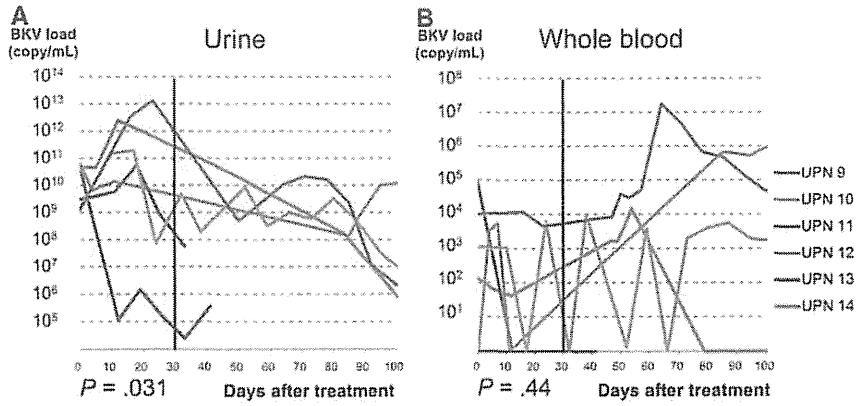


**Figure 2.** BK virus (BKV) load after choreito treatment. The BKV load before treatment amounted to a median of $2.6 \times 10^{10}$ copies/mL in urine (range, $1.3 \times 10^{9}$ to $6.3 \times 10^{10}$ copies/mL) and a median of $6.5 \times 10^{2}$ copies/mL in whole blood (range, 0 to $9.0 \times 10^{4}$ copies/mL). The median urine BKV load was $1.7 \times 10^{8}$ copies/mL (range, $2.6 \times 10^{4}$ to $3.1 \times 10^{10}$ copies/mL) 1 month after BKV-HC diagnosis, and the BKV load had significantly decreased since the time of diagnosis (Wilcoxon signed-rank test, $P = .031$) (A). The BKV load in whole blood appeared stable during the course of BKV-HC, and no significant decrease was observed a month after diagnosis (Wilcoxon signed-rank test, $P = .44$) (B).

confirmed in children. Fluoroquinolones are historically contraindicated in children because they cause arthrotoxicity in juvenile animals and are associated with reversible musculoskeletal events in both children and adults; therefore, they are not recommended in the absence of convincing evidence.

Choreito is a formula stemming from Japanese traditional (Kampo) medicine, originally developed from traditional Chinese medicine; it was the orthodox medicine in Japan until the 19th century, when modern Western medicine took over [14]. Nevertheless, some Kampo formulae are still officially registered in the Japanese Pharmacopoeia. Although Kampo extracts are crude drugs derived from plants, animals, and minerals, their quality is strictly controlled in accordance with the Japanese Pharmacopoeia by quantitative analysis of marker components using high-performance liquid chromatography. Kampo formulae are classified as dietary supplements outside Japan and are approved for marketing by the Food and Drug Administration in the United States.

Choreito is a crude product from *Polyporus umbellatus* sclerotium, *Wolfiporia extensa* sclerotium, *Alisma orientale* rhizome, aluminum silicate hydrate with silicon dioxide, and glue. Ergone isolated from *P. umbellatus* prevented early renal injury in a rat model of nephropathy [23] and may play a central role in the effect exerted by choreito. Pollakisuria was ameliorated in 93% of patients who received choreito for lower urinary tract symptoms in an open-label, single-arm study of 30 patients [24]. Choreito was also administered to patients with urolithiasis for enhancing the evacuation of stones after extracorporeal shock wave lithotripsy [25]. In these studies, no severe adverse effects were observed, suggesting high safety of choreito.

Considering the wide range of indications in genitourinary disorders, choreito may protect epithelial cells irrespective of the type of pathogens and thereby be an effective treatment option for the hemostasis of HC. Although the precise pathogenesis of BKV-HC remains unclear, urothelial cells infected with BKV in vitro detached without causing local cell lysis, which may be associated with the denudation of the damaged mucosa in patients with BKV-HC [26]. Choreito may protect urothelial cells from detaching, which may result in a significant reduction of the BKV load in urine, although the whole blood BKV load appears unchanged and the BKV burden itself is not reduced. Notably, unlike other antiviral agents or surgical interventions, no adverse effects were observed during choreito administration, although the mechanism of action of choreito remains unclear; hence, its safety cannot be easily predicted.

Our study has some limitations. The small number of study subjects in this single-center retrospective analysis may result in bias. Five of 8 subjects in the nonchoreito group had grade II to III GVHD, whereas 1 out of 6 subjects in the choreito group had grade IV GVHD. This difference in GVHD frequency could have been a contributing factor for the difference in HC severity and BKV clearance, although it was not statistically different ($P = .14$) among the 2 groups, possibly because of the small sample size. Children with concomitant AdV viruria were included only in the nonchoreito group, which may explain the longer time before CR in the nonchoreito group. In the present study, HC was significantly more severe in the choreito group than the nonchoreito group. This difference may represent the difference in preconditioning and donor sources: the choreito group included more cases of haplo-identical HSCT, which may have resulted in intensified immunosuppression. More severe HC correlates with a longer duration of HC [2]. Nevertheless, the duration of HC was significantly shorter in the choreito group, which exemplifies its effectiveness. Although the urine BKV load had significantly decreased 1 month after choreito treatment examined by the paired samples, this decrease could not be compared with that of the nonchoreito group because of a lack of paired samples in most of the patients in the nonchoreito group. Thus, the impact of choreito treatment on the urine BV virus load should be investigated in a prospective study where the BKV load is sequentially followed for every study subject.

In conclusion, choreito may be a safe and effective therapy for the hemostasis of late-onset BKV-HC following HSCT, although it may not decrease the BKV burden. Although its precise mechanism of hemostasis remains unclear, choreito may be administered as the first-line treatment for post-HSCT HC. Prospective, randomized studies are warranted to confirm the efficacy of choreito in the treatment of BKV-HC. Fundamental research aiming to identify the active ingredients and mechanisms of action is also essential.

## ACKNOWLEDGMENTS

The authors thank Fumiyo Ando, Yoshie Miura, Yinyan Xu, and Xinan Wang for their professional assistance.

*Financial disclosure:* Dr. Seiji Kojima received a research grant from Sanofi K.K. The other authors have no conflicts of interest to disclose.

## SUPPLEMENTARY DATA

Supplementary data related to this article can be found online at http://dx.doi.org/10.1016/j.bbmt.2014.10.018.

## REFERENCES

1. Lee YJ, Zheng J, Kolitsopoulos Y, et al. Relationship of BK polyoma virus (BKV) in the urine with hemorrhagic cystitis and renal function in recipients of T cell-depleted peripheral blood and cord blood stem cell transplantations. *Biol Blood Marrow Transplant*. 2014;20:1204-1210.
2. Gilis L, Morisset S, Billaud G, et al. High burden of BK virus-associated hemorrhagic cystitis in patients undergoing allogeneic hematopoietic stem cell transplantation. *Bone Marrow Transplant*. 2014;49:664-670.
3. Haines HL, Laskin BL, Goebel J, et al. Blood, and not urine, BK viral load predicts renal outcome in children with hemorrhagic cystitis following hematopoietic stem cell transplantation. *Biol Blood Marrow Transplant*. 2011;17:1512-1519.
4. Decker DB, Karam JA, Wilcox DT. Pediatric hemorrhagic cystitis. *J Pediatr Urol*. 2009;5:254-264.
5. Megged O, Stein J, Ben-Meir D, et al. BK-virus-associated hemorrhagic cystitis in children after hematopoietic stem cell transplantation. *J Pediatr Hematol Oncol*. 2011;33:190-193.
6. Oshrine B, Bunin N, Li Y, et al. Kidney and bladder outcomes in children with hemorrhagic cystitis and BK virus infection after allogeneic hematopoietic stem cell transplantation. *Biol Blood Marrow Transplant*. 2013;19:1702-1707.
7. Laskin BL, Denburg M, Furth S, et al. BK viremia precedes hemorrhagic cystitis in children undergoing allogeneic hematopoietic stem cell transplantation. *Biol Blood Marrow Transplant*. 2013;19:1175-1182.
8. Cesaro S, Facchin C, Tridello G, et al. A prospective study of BK-virus-associated haemorrhagic cystitis in paediatric patients undergoing allogeneic haematopoietic stem cell transplantation. *Bone Marrow Transplant*. 2008;41:363-370.
9. Kloos RQ, Boelens JJ, de Jong TP, et al. Hemorrhagic cystitis in a cohort of pediatric transplantations: incidence, treatment, outcome, and risk factors. *Biol Blood Marrow Transplant*. 2013;19:1263-1266.
10. Drew RJ, Walsh A, Ní Laoi B, et al. BK virus (BKV) plasma dynamics in patients with BKV-associated hemorrhagic cystitis following allogeneic stem cell transplantation. *Transpl Infect Dis*. 2013;15:276-282.
11. Savva-Bordalo J, Pinho Vaz C, Sousa M, et al. Clinical effectiveness of hyperbaric oxygen therapy for BK-virus-associated hemorrhagic cystitis after allogeneic bone marrow transplantation. *Bone Marrow Transplant*. 2012;47:1095-1098.
12. Zaman RA, Ettenger RB, Cheam H, et al. A novel treatment regimen for BK viremia. *Transplantation*. 2014;97:1166-1171.

13. Harkensee C, Vasdev N, Gennery AR, et al. Prevention and management of BK-virus associated haemorrhagic cystitis in children following haematopoietic stem cell transplantation—a systematic review and evidence-based guidance for clinical management. *Br J Haematol*. 2008;142:717-731.
14. Kawashima N, Deveaux TE, Yoshida N, et al. Choreito, a formula from Japanese traditional medicine (Kampo medicine), for massive hemorrhagic cystitis and clot retention in a pediatric patient with refractory acute lymphoblastic leukemia. *Phytomedicine*. 2012;19:1143-1146.
15. Droller MJ, Gomolka D. Expression of the cellular immune response during tumor development in an animal model of bladder cancer. *J Urol*. 1982;128:1385-1389.
16. Funahashi Y, Iwata S, Ito Y, et al. Multiplex real-time PCR assay for simultaneous quantification of BK polyomavirus, JC polyomavirus, and adenovirus DNA. *J Clin Microbiol*. 2010;48:825-830.
17. Hale GA, Rochester RJ, Heslop HE, et al. Hemorrhagic cystitis after allogeneic bone marrow transplantation in children: clinical characteristics and outcome. *Biol Blood Marrow Transplant*. 2003;9:698-705.
18. Hassan Z. Management of refractory hemorrhagic cystitis following hematopoietic stem cell transplantation in children. *Pediatr Transplant*. 2011;15:348-361.
19. Gorczynska E, Turkiewicz D, Rybka K, et al. Incidence, clinical outcome, and management of virus-induced hemorrhagic cystitis in children and adolescents after allogeneic hematopoietic cell transplantation. *Biol Blood Marrow Transplant*. 2005;11:797-804.
20. Kwon HJ, Kang JH, Lee JW, et al. Treatment of BK virus-associated hemorrhagic cystitis in pediatric hematopoietic stem cell transplant recipients with cidofovir: a single-center experience. *Transpl Infect Dis*. 2013;15:569-574.
21. Cesaro S, Hirsch HH, Faraci M, et al. Cidofovir for BK virus-associated hemorrhagic cystitis: a retrospective study. *Clin Infect Dis*. 2009;49:233-240.
22. Zama D, Masetti R, Vendemini F, et al. Clinical effectiveness of early treatment with hyperbaric oxygen therapy for severe late-onset hemorrhagic cystitis after hematopoietic stem cell transplantation in pediatric patients. *Pediatr Transplant*. 2013;17:86-91.
23. Zhao YY, Zhang L, Mao JR, et al. Ergosta-4,6,8(14),22-tetraen-3-one isolated from Polyporus umbellatus prevents early renal injury in aristolochic acid-induced nephropathy rats. *J Pharm Pharmacol*. 2011;63:1581-1586.
24. Horii A, Maekawa M. Clinical evaluation of chorei-to and chorei-to-go-shimotsu-to in patients with lower urinary tract symptoms [article in Japanese]. *Hinyokika Kiyo*. 1988;34:2237-2241.
25. Wada S, Yoshimura R, Yamamoto K, et al. Effect of herbal drug, choreito, after extracorporeal shock wave lithotripsy on spontaneous stone delivery. *Jpn J Endourol ESWL*. 2001;14:155-158.
26. Li R, Sharma BN, Linder S, et al. Characteristics of polyomavirus BK (BKPyV) infection in primary human urothelial cells. *Virology*. 2013;440:41-50.

# Establishment of a Humanized APL Model via the Transplantation of *PML-RARA*-Transduced Human Common Myeloid Progenitors into Immunodeficient Mice

**Hiromichi Matsushita[1,2,3]*, Takashi Yahata[1,2,4], Yin Sheng[1], Yoshihiko Nakamura[1], Yukari Muguruma[1], Hideyuki Matsuzawa[1,5], Masayuki Tanaka[5], Hideki Hayashi[5], Tadayuki Sato[5], Anar Damdinsuren[3], Makoto Onizuka[6], Mamoru Ito[7], Hayato Miyachi[3], Pier Paolo Pandolfi[8], Kiyoshi Ando[1,2,6]***

1 Research Center for Cancer Stem Cell, Tokai University School of Medicine, Isehara, Kanagawa, Japan, 2 Medical Research Institute, Tokai University, Isehara, Kanagawa, Japan, 3 Department of Laboratory Medicine, Tokai University School of Medicine, Isehara, Kanagawa, Japan, 4 Department of Cell Transplantation, Tokai University School of Medicine, Isehara, Kanagawa, Japan, 5 Support Center for Medical Research and Education, Tokai University, Isehara, Kanagawa, Japan, 6 Division of Hematology and Oncology, Department of Internal Medicine, Tokai University School of Medicine, Isehara, Kanagawa, Japan, 7 Central Institute for Experimental Animals, Kawasaki, Kanagawa, Japan, 8 Cancer Research Institute, Beth Israel Deaconess Cancer Center, Departments of Medicine and Pathology, Beth Israel Deaconess Medical Center, Harvard Medical School, Boston, Massachusetts, United States of America

## Abstract

Recent advances in cancer biology have revealed that many malignancies possess a hierarchal system, and leukemic stem cells (LSC) or leukemia-initiating cells (LIC) appear to be obligatory for disease progression. Acute promyelocytic leukemia (APL), a subtype of acute myeloid leukemia characterized by the formation of a PML-RARα fusion protein, leads to the accumulation of abnormal promyelocytes. In order to understand the precise mechanisms involved in human APL leukemogenesis, we established a humanized *in vivo* APL model involving retroviral transduction of *PML-RARA* into $CD34^+$ hematopoietic cells from human cord blood and transplantation of these cells into immunodeficient mice. The leukemia well recapitulated human APL, consisting of leukemic cells with abundant azurophilic abnormal granules in the cytoplasm, which expressed CD13, CD33 and CD117, but not HLA-DR and CD34, were clustered in the same category as human APL samples in the gene expression analysis, and demonstrated sensitivity to ATRA. As seen in human APL, the induced APL cells showed a low transplantation efficiency in the secondary recipients, which was also exhibited in the transplantations that were carried out using the sorted $CD34^-$ fraction. In order to analyze the mechanisms underlying APL initiation and development, fractionated human cord blood was transduced with *PML-RARA*. Common myeloid progenitors (CMP) from $CD34^+/CD38^+$ cells developed APL. These findings demonstrate that CMP are a target fraction for *PML-RARA* in APL, whereas the resultant $CD34^-$ APL cells may share the ability to maintain the tumor.

**Citation:** Matsushita H, Yahata T, Sheng Y, Nakamura Y, Muguruma Y, et al. (2014) Establishment of a Humanized APL Model via the Transplantation of *PML-RARA*-Transduced Human Common Myeloid Progenitors into Immunodeficient Mice. PLoS ONE 9(11): e111082. doi:10.1371/journal.pone.0111082

**Editor:** Marina Konopleva, University of Texas M.D. Anderson Cancer Center, United States of America

**Received** February 27, 2014; **Accepted** September 24, 2014; **Published** November 4, 2014



**Funding:** Hiromichi Matsushita received funding from a Grant-in-Aid for Scientific Research from The Ministry of Education, Culture, Sports, Science and Technology of Japan (#24591411, URL http://www.jsps.go.jp/english/e-grants/), Tokai University School of Medicine Project Research (http://www.med.u-tokai.ac.jp/web/international/about_us/message_from_the_dean.html), and the Takeda Science Foundation (http://www.takeda-sci.or.jp/index.html). Kiyoshi Ando received support from a Grant-in-Aid for Scientific Research from The Ministry of Education, Culture, Sports, Science and Technology of Japan (#24390248). The funders had no role in study design, data collection and analysis, decision to publish, or preparation of the manuscript.

**Competing Interests:** The authors have declared that no competing interests exist.

* Email: hmatsu@is.ic.cc.u-tokai.ac.jp (H. Matsushita); andok@keyaki.cc.u-tokai.ac.jp (KA)

## Introduction

Acute myeloid leukemia (AML) constitutes a heterogeneous group of tumors in myeloid lineage cells characterized by the proliferation and accumulation of immature myeloblasts [1]. Recent advances in cancer biology have revealed that various genetic events result in the blockage of differentiation with subsequent uncontrolled cellular proliferation. In addition, *in vivo* analyses using a xenograft model with immunodeficient mice have shown that a very immature subset of AML cells called leukemic stem cells (LSC), which are typically characterized as $CD34^+/CD38^-$ cells, as observed in normal hematopoietic stem cells (HSCs), have been shown to slowly undergo cell division to both yield progenitor cells and sustain the LSC population, thus resulting in the maintenance of the tumor [2–6]. More recently, several reports have shown that $CD34^+/CD38^+$ hematopoietic progenitors are able to acquire the ability to maintain populations of LSC or leukemia-initiating cells (LIC) [7]. It is therefore possible that the phenotypes of LIC differ among the subtypes of AML.

Acute promyelocytic leukemia (APL) is a subset of AML defined by the formation of a chimeric gene, promyelocytic leukemia-retinoic acid receptor α (*PML-RARA*) [8]. It is characterized by the accumulation of abnormal promyelocytes with abundant large azurophilic granules, suggesting that APL cells undergo maturation arrest in the later steps of myeloid differentiation. The typical pattern of cellular surface markers of APL is positive for CD13,

CD33 and CD117, and negative for CD34, which is usually presumed to indicate cellular immaturity, and HLA-DR [9]. It is very difficult to engraft primary APL samples in immunodeficient mice. They did not become engrafted into the NOD/SCID mice to any degree [3]. In NOD/Shi-SCID/IL-2Rγ$^{null}$ (NOG) mice, which are more profoundly immunocompromised than NOD/SCID mice [10,11], six out of eight APL samples were not engrafted or only very little engrafted [12]. It is therefore possible that the mechanisms underlying the development of APL differ from those involved in the pathogenesis of AML uncovered to date. Elucidating the pathogenesis of APL is important for improving the treatment of APL patients, and will provide clues to understand the development of other subtypes of AML.

*In vivo* analyses using transgenic APL mice models with *PML-RARA* have revealed that a population of committed myeloid progenitor cells (CD34$^+$, c-kit$^+$, FcγRIII/II$^+$, Gr1$^{int}$) was identified as the APL-LIC [13,14]. However, the cellular surface antigens and the gene expression pattern in humans are different from those in mice. In particularly, in transgenic systems, murine APL developed after a long latent period through a myelodysplastic/proliferative phase, which does not usually precede human APL [15–18]. There have been no *in vivo* models for exploring leukemogenesis of human APL to date; largely because human primary APL cells are difficult to engraft as a xenograft [3,12]. *PML-RARA*-retrovirally transduced human CD34$^+$ cells from cord blood have therefore only been evaluated *in vitro* [19].

Therefore, the aim of this study was to establish a humanized xenograft APL model using the retroviral transduction of *PML-RARA* into human CD34$^+$ cells and NOG mice in order to investigate the mechanisms of APL leukemogenesis, such as that involving disease initiation and maintenance in the model.

## Materials and Methods

### Fractionation of human hematopoietic cells from cord blood

Cord blood (CB) and patients' APL samples were obtained after written informed consent was provided in accordance with the Declaration of Helsinki and with approval from the Tokai University Committee on Clinical Investigation (Permit number: #12I-46 and #12I-49). CD34 positive and negative specimens were primarily prepared using the CD34 Progenitor Cell Isolation Kit (Miltenyi Biotec, Bergisch Gladbach, Germany). CD34$^+$ cells were then purified again using anti-human CD34 mAbs (Beckman Coulter, Brea, CA), in combination with or without an anti-CD38 antibody (BD, Franklin Lakes, NJ), with a FACS vantage instrument (BD). CD34$^-$/CD33$^+$ cells were also purified again using anti-human CD34 and CD33 mAbs (Beckman Coulter) and the FACS vantage instrument. The preparation of common myeloid progenitors (CMP), granulocyte-monocytic progenitors (GMP) and megakaryocyte-erythrocyte progenitors (MEP) was performed using an anti-CD123 antibody (BD) and anti-CD45RA (Biolegend, San Diego, CA) antibody, according to a previous report [20].

### Retrovirus transduction of *PML-RARA* into human hematopoietic cells

The MIGR1 retroviral vector [21] or MIGR1-*PML-RARA* (bcr3/short form) [22] in combination with the vesicular stomatitis virus-G protein (VSV-G) envelope vector (pCMV-VSV-G) was transiently transfected into PLAT-gp cells using the Fugene 6 transfection reagent (Roche Diagnostics, Basel, Switzerland). The culture supernatant was concentrated 100 to 200 times by ultracentrifugation. After overnight culture of the fractionated cells in StemPro-34 (Life Technologies, Carlsbad, CA) with TPO, SCF, and FLT3 ligand (50 ng/ml each), they were incubated with the concentrated supernatant on retronectin-coated plates (Takara-Bio, Otsu, Japan). Retroviral transduction was performed twice, and then transplantation was performed the next day.

### Colony-forming unit-cells assay

*PML-RARA* transduced cells were sorted by their EGFP, CD34 and CD38 expression by FACS vantage 48 h after infection. The colony-forming unit-cells (CFU-C) assay was performed as described previously [23]. The fluorescent images were captured using a HS All-in-One Fluorescence Microscope Biorevo 9000 (Keyence Corporation, Osaka, Japan) and were analyzed by the BZ II software program (Keyence Corporation).

### RNA extraction and RT-PCR

Total RNA was isolated using the RNeasy micro kit (Qiagen, Hilden, Germany) or Isogen (Nippon gene, Tokyo, Japan), and the reverse-transcribed cDNA was amplified by qualitative PCR. The qualitative-PCR analysis was performed by SRL Inc. (Hachioji, Tokyo, Japan). The sequences of PCR primers and probes were shown in **Table S1**.

### Transplantation, serial transplantation and ATRA treatment

Nine- to 20-week-old NOD/Shi-scid, IL-2Rγc$^{null}$ (NOG) mice [10,11] were irradiated with 220 cGy of X-rays. On the following day, the whole infected cells or primary AML cells were intravenously injected. The EGFP-positive cells in the peripheral blood were monitored. The mice with induced APL were defined as those bearing more than 0.1% EGFP$^+$ cells which dominantly expressed CD33 (more than 70%) in their bone marrow at four months after transplantation. In the initial analysis, the occurrence of APL was confirmed by the morphological observations using cytospin slides after EGFP sorting. For serial transplantation, bone marrow cells were obtained from recipient mice, and the sorted EGFP-positive cells were injected intravenously or intramedullary into the irradiated mice [24]. The engrafted mice were treated intraperitoneally with 1.5 μg/g of body weight/day of all-*trans* retinoic acid (ATRA, Sigma) for 21 days [25], and were then sacrificed to collect the EGFP-positive cells in the bone marrow by sorting. All the experiments using animals were approved by the animal care committee of Tokai University (Permit number: #132028).

### Flow cytometric analysis

The cells were stained with APC-conjugated anti-human CD45, CD33, CD34, HLA-DR (Beckman Coulter), CD13, and CD117 (BD) mAbs. They were subjected to flow cytometry using a FACSCalibur instrument (BD) and the CellQuest software program (BD).

### Cell preparation, Wright-Giemsa staining and immunofluorescence microscopy

Cytospin slides were prepared using a Cytospin 4 Cytocentrifuge (Thermo Scientific, Waltham, MA) at 500 rounds per minute for 5 min. To observe the cellular morphology, Wright-Giemsa staining was performed. For the immunofluorescent study, cells were seeded onto poly-L-lysine coated slides and fixed with ice cold 70% ethanol for 15 min. After permeabilization with 0.2% Triton X-100 for 20 min, the slides were treated with PBS containing 5% normal goat serum for 1 hour to block the nonspecific binding of antibodies. The anti-PML antibody (Merck

Millipore, Billerica, MA) was applied overnight at 4°C. Cells were counterstained with DAPI. Images were captured with an LSM510 META confocal microscope (Carl Zeiss, Oberkochen, Germany) and processed using Adobe Photoshop 7.0 (Adobe Systems, San Jose, CA).

### Southern blot analysis

Genomic DNA was extracted from the cells using a DNeasy kit (Qiagen). Ten micrograms of the DNA were electrophoresed and transferred to nylon membranes (Hybond-N+, GE Healthcare, Fairfield, CT). The DNA was then crosslinked to the membrane by ultraviolet light. The EGFP probe was prepared from MIGR1 vector by cutting it using NcoI and SalI, and was labeled with $^{32}$P-dCTP using the Rediprime II DNA Labelling System (GE Healthcare). The membrane was hybridized with the probe in Rapid-hyb buffer (GE Healthcare), and was analyzed by a Phosphoimager (LAS1000, Fuji Film, Tokyo, Japan).

### Microarray

Total RNA was labeled and hybridized to Affymetrix Human Genome U133 Plus 2.0 Array GeneChip microarrays (Affymetrix, Santa Clara, CA) using the manufacturer's protocols. The results were deposited in the Gene Expression Omnibus (GEO; http://www.ncbi.nlm.nih.gov/geo/; accession no. GSE49344). The microarray data from normal human promyelocytes and clinical samples bearing AML, including APL, were obtained from the deposited data on the GEO (GSE12662). The APL-specific expressed genes have been described in detail in a previous study [26]. The probe set data were generated using standard normalization algorithms included in the Affymetrix Microarray Suite software program, v.5 (MAS5.0). The clustering analysis was performed by the Gene spring GX software program, version 11 (Agilent technology, Santa Clara, CA).

To identify the genes that are differentially expressed in a specific cellular subset, all probe sets with fewer than 10% present calls in both groups and a coefficient of variation <0.5 across all samples were eliminated prior to the subsequent analysis; (i) The genes differently expressed in the induced APL cases among the AML cases were defined as genes whose expression change (upregulation or downregulation) was ≥2.0 fold in comparison to those in AML other than APL, (ii) The genes associated with immaturity in the induced APL cases were expressed at significantly higher levels in CD34$^+$ cells than the other normal cells (FDR <0.05, fold-change >2.0 upregulated), and were also expressed in the induced APL cells at similar levels (induced APL: CD34$^+$ ≥1:1), and moreover, these genes were expressed at higher levels in promyelocytes (induced APL: Pros ≥2:1). (iii) The genes upregulated during promyelocyte differentiation were expressed at significantly higher levels in promyelocytes than in the other normal cells (FDR <0.05, fold-change >2.0 upregulated), and were expressed at lower levels in the induced APL (induced APL: Pros ≤1:2), (iv) The genes induced by *PML-RARA* were expressed at higher levels in the induced APL than in all the normal cells (induced APL: normal ≥2:1), and were not expressed in any normal cells (more than 75% absent calls, as summarized by the MAS5.0). Statistical significance was assessed by the unpaired unequal variance Welch test (P<0.05), and correction for multiple testing was performed by the Benjamini and Hochberg False Discovery Rate (FDR), using a cutoff of 0.05.

The gene set specific for induced APL was defined to fulfill one or more of the above criteria (ii) to (iv) in the gene set identified in (i).

### The integration site analysis of *PML-RARA* using linear amplification-mediated PCR

To identify the genomic-proviral junction sequence, linear amplification-mediated polymerase chain reaction (LAM-PCR) was performed as described previously, with minor modifications [27,28]. In brief, genomic DNA from bone marrow cells was first digested with Tsp509I. A linear amplification of target DNA in the digested genome was performed by repeated primer extension using a vector-specific 5′-biotinylated primer, LTR1.5, and Taq polymerase. After selection with Dynabeads MyOne Streptavidin C1 (Life Technologies), a double-stranded asymmetrical linker cassette was ligated to the Tsp509I-digested site using T4 DNA Ligase. The DNA products were then amplified by PCR using a vector-specific primer, LTR3, and linker cassette primer, LC1. The nested PCR was performed using internal primers LTR5 and LC2. The final products were sequenced after cloning them into the TOPO TA cloning vector (Life Technologies). The primer sequences are shown in **Table S1**.

### Statistical analyses

The Kaplan-Meier method was used to estimate the leukemia-free survival (LFS) of mice. Log-rank p values were used for comparisons of the LFS among three subgroups. The analyses were conducted using the GraphPad Prism software package (GraphPad Software, La Jolla, CA). The other statistical analyses were performed using the Mann-Whitney U Test with the IBM SPSS Statistics software program (New York, NY). Values of $p < 0.05$ were considered to be statistically significant.

## Results

### Functions of PML-RARα in human CD34 cells *in vitro*

To examine the functions of PML-RARα *in vitro*, a MIGR1-*PML-RARA* or MIGR1 control vector was retrovirally infected into human CD34$^+$ cells from cord blood. The transduction efficiency evaluated by EGFP positivity was 0.5% to 18.6% (n = 10, median: 5.7%) and 2.1% to 19.7% (n = 25, median: 6.8%), respectively. The expression of *PML-RARA* in these cells was confirmed by RT-PCR (**Figure S1**). The induction of *PML-RARA* in CD34$^+$ cells disrupted PML nuclear bodies by interacting with wild-type PML via the PML portion of the chimeric transcript, and the distribution of PML in the nucleus was altered to show a microspeckled pattern in these cells [29–31] (**Figure 1A**). Additionally, the induction of *PML-RARA* reduced all the colony formation capacity (**Figure 1B**). The *PML-RARA* expression was confirmed in these colonies by EGFP fluorescence (**Figure S1 and S2**) and RT-PCR, although the expression levels were 37 times lower compared to those in the CD34$^+$ cells 48 hours after *PML-RARA* transduction (**Figure S3**). Regarding the content of colonies, MIGR1-infected CD34$^+$ cells mainly generated the erythroid lineage-containing colonies, such as CFU-mix and BFU-E, whereas more than half of the colonies from the CD34$^+$ cells with *PML-RARA* were of the myeloid lineage, like CFU-GM (**Figures 1C**). These data demonstrate that *PML-RARA* induces the myeloid commitment of human CD34$^+$ cells.

### Establishment of a humanized *in vivo* APL model

The cells transduced with *PML-RARA* or the MIGR1 control vector were then transplanted into NOG mice. The EGFP$^+$ cells survived and proliferated three to four months after transplantation only in the NOG mice transplanted with *PML-RARA*-, not control vector at all, infected human CD34$^+$ cells. The median proportion of EGFP$^+$/CD45$^+$ cells in the bone marrow obtained from the transplanted mice was 23.7% (0.95% to 96.5%, n = 24)

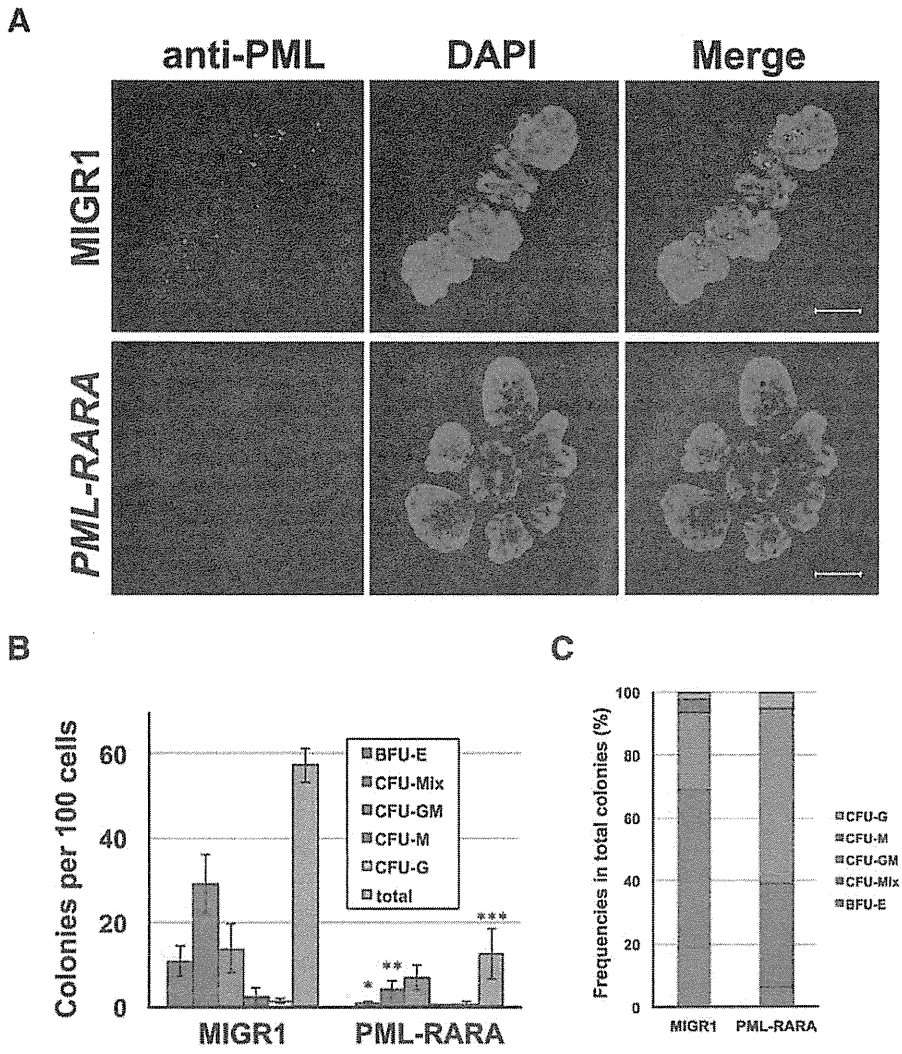


**Figure 1. The function of *PML-RARA* in human CD34$^+$ cells *in vitro*.** (**A**) The results of an immunofluorescent analysis of PML distribution in human CD34$^+$ cells transduced with *PML-RARA*. The images were captured with an LSM510 META confocal microscope (Carl Zeiss). The bars indicate 10 μm. (**B**) The colony-forming assay using *PML-RARA*-transduced CD34$^+$ cells. The cells were sorted by EGFP expression 48 h after infection. Colony formation was evaluated on days 10 to 12 after plating the cells. The average numbers of colonies from three independent experiments are shown. Data represent the means ± SD. The asterisks (*) indicate $p<0.05$. (**C**) The proportion of each kind of colony was calculated from the results of the colony-forming assay shown in (B). The percentages of CFU-GM are higher in *PML-RARA*-infected cells than in control (MIGR1) cells ($p=0.013$).
doi:10.1371/journal.pone.0111082.g001

(**Figure 2A**). The majority of the engrafted EGFP$^+$/human CD45$^+$ cells expressed human CD33 (70.2% to 100%, median 90.6%, n = 24) (**Figure 2B**), thus suggesting that they were of the myeloid lineage. The *PML-RARA* expression was detected only in the EGFP$^+$ fraction and not in the EGFP$^-$ fraction of the sorted human CD45$^+$/CD33$^+$ cells from the NOG mice (**Figure 2C**). The expression levels of *PML-RARA* were decreased about 17-fold in comparison to those in the CD34$^+$ cells 48 hours after *PML-RARA* transduction (**Figure S3**), but the presence of *PML-RARA* in the human myeloid cells, recognized as EGFP$^+$ cells, caused marked accumulation of promyelocytes, in comparison to the control EGFP$^-$ human myeloid cells (52.8% in EGFP$^+$ cells vs 19.4% EGFP$^-$ cells in the 13 paired samples, $p<0.0001$). On the other hand, the proportions of myeloblasts, mature neutrophils and monocytes were decreased (5.2% vs 14.4%, $p=0.010$; 2.5% vs 12.7%, $p=0.005$; 4.0% vs 10.1%, $p=0.016$) (**Figure 2D**). These findings confirmed that the expression of *PML-RARA* induced the myeloid differentiation of human CD34$^+$ cells and blocked them at the promyelocytic stage. Morphologically, the promyelocytes had abundant large azurophilic granules and round nuclei with a high nucleocytoplasmic ratio. Some of them had a number of Auer bodies and looked like Faggot cells, which are the typical morphological features of APL cells, and were not seen in the previous murine models (**Figure 2E**). A Southern blot analysis using an EGFP probe revealed that the EGFP$^+$/CD45$^+$/CD33$^+$ cells oligoclonally proliferated *in vivo* (**Figure 2F**).

The induced APL cells were detected in 24 out of the 34 mice (71%) transplanted with *PML-RARA*-transduced CD34 cells ($p=0.0184$ in comparison to the control). They were detected in all 16 mice when the calculated number of the transplanted EGFP$^+$/CD34$^+$ cells per mouse was more than 3,000 (4,655 to 29,728 cells, median: 11,085 cells) ($p=0.0006$ in comparison to the control). On the other hand, they were only detected in eight out of 18 mice (44%) transplanted with EGFP$^+$/CD34$^+$ cells at a

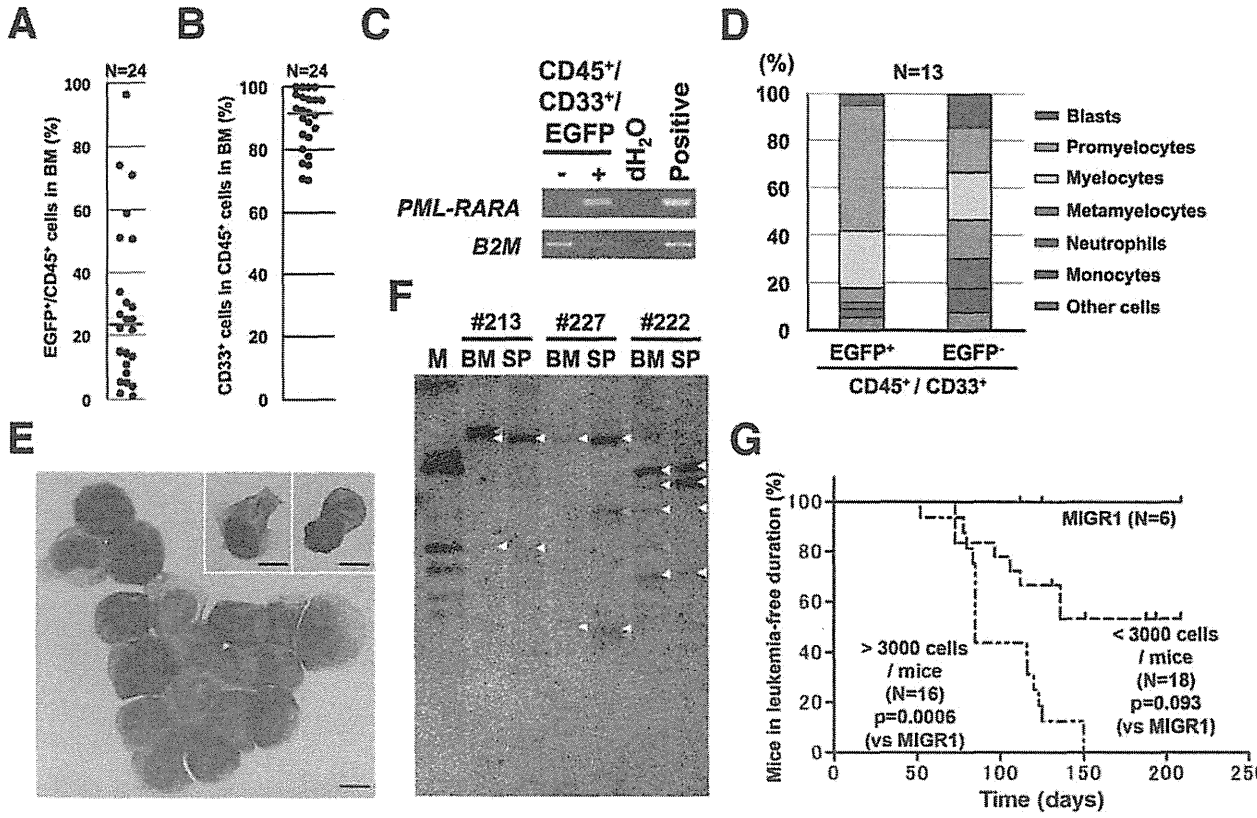


**Figure 2. Establishment of humanized APL *in vivo*.** (**A**) The proportion of EGFP$^+$/human CD45$^+$ cells in the bone marrow of leukemic NOG mice. Each dot represents a single mouse. The horizontal line represents the median value. (**B**) The proportion of CD33$^+$ cells among the EGFP$^+$/human CD45$^+$ cells in the bone marrow of the leukemic NOG mice. Each dot represents a single mouse. The horizontal line represents the median value. (**C**) The expression of *PML-RARA* in RT-PCR was detected only in the EGFP$^+$ fraction obtained from the engrafted human CD45$^+$/CD33$^+$ cells. The cells were obtained from bone marrow 16 weeks after transplantation. *B2M, beta 2 microglobulin*. The *PML-RARA* expression vector and human CD34$^+$ cells were used as a positive control for the *PML-RARA* and *B2M* analysis, respectively. (**D**) The differential counts of the engrafted CD45$^+$/CD33$^+$/EGFP$^+$ and EGFP$^-$ cells from the mice transplanted with *PML-RARA*-induced human CD34$^+$ cells. They were obtained from bone marrow 16 to 20 weeks after transplantation. The data represent the means. (**E**) A representative photograph of the resulting leukemic cells which morphologically recapitulated APL. Faggot cells were recognized, as seen in the right top corner. The images were captured with a BX41 microscope (Olympus). The bar indicates 10 μm. (**F**) The results of a Southern blot analysis of the genomic DNA from induced APL cells with an EGFP probe. Clonal bands are shown by arrow heads: white, seen in both BM and SP; orange, seen only in BM or SP. BM, bone marrow; SP, spleen. (**G**) The leukemia-free duration in NOG mice transplanted with *PML-RARA*-transduced CD34$^+$ cells.
doi:10.1371/journal.pone.0111082.g002

density of less than 3,000 (480 to 2,660 cells, median: 1,861 cells) ($p = 0.093$ in comparison to the control) (**Figure 2G**). This proportion was not dependent on the number of transplanted EGFP$^+$/CD34$^+$ cells.

These findings demonstrate that a humanized APL model can be successfully established by the transplantation of *PML-RARA*–transduced human CD34 cells into NOG mice.

## Characteristics of the induced APL cells obtained from the humanized *in vivo* model

The induced APL cells were positive for human myeloid markers such as CD13, CD33 and CD117, and were negative for CD34 and HLA-DR, as seen in typical human APL [32]. *PML-RARA* did not contribute to the development of lymphocytes. Human CD19$^+$ B-cells in the spleen and human CD4$^+$/CD8$^+$ T-cells in the thymus were negative for EGFP (**Figure 3A**).

To evaluate the gene expression of the induced APL cells, a microarray analysis was performed, and the expression of the 510 APL-specific genes identified in a previous study was compared with that observed in the clinical AML samples [26]. Two clinical APL samples from our patients were simultaneously evaluated and were aligned in the APL category defined in the study, suggesting that our microarray results were comparable with those in the previous study. The induced APL cells from our models were also classified into the APL category when compared to normal promyelocytes and AML samples other than APL (**Figure 3B**).

In common with this previous study [26], the 3,439 probes (3278 genes) differentially expressed in the induced APL and the AML other than APL ((i) in the Materials and Methods) grouped the induced APL and human primary APL together, separately from the other types of AML (**Figure S4**). The gene sets whose expression in the induced APL cases was not dependent on the myeloid differentiation were also filtered by comparison with the data for normal myeloid cells. They included the genes for immaturity expressed in the induced APL (1,782 probes, including 1,720 genes), the genes upregulated in promyelocyte differentiation not in the induced APL (447 probes, including 427 genes) and the genes specifically induced by *PML-RARA* (466 probes, including 429 genes) ((ii), (iii) and (iv) in the Materials and Methods). Each gene set was analyzed using the DAVID website

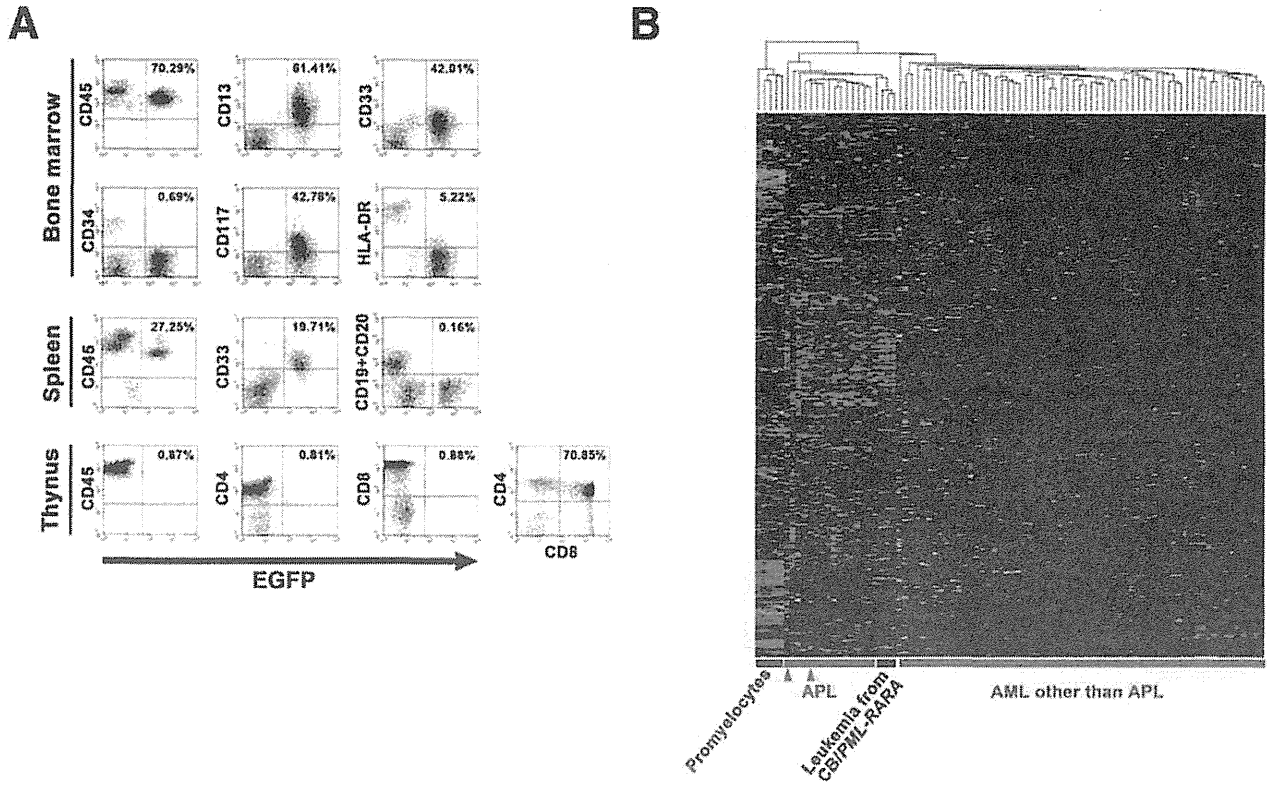


**Figure 3. Characteristics of the induced APL *in vivo*.** (**A**) The representative expression pattern of cell surface markers in the induced APL cells determined by a flow cytometric analysis. All the scatter plots show the relationships between the EGFP positivity and cell surface marker expression. The whole living cells gated as a propidium iodide-negative fraction in the bone marrow were analyzed. The induced APL cells were recognized as $EGFP^+$ cells. A few murine hematopoietic cells, recognized as a human $CD45^-$ fraction, were detected in this mouse. (**B**) The heat map of the microarray analysis using the 510 APL-specific genes for the comparison of the induced APL cells (purple, n = 3) with APL (red, n = 16), other types of AML (M0, 1, 2 and 4 in FAB classification, green, n = 62) and normal promyelocytes (blue, n = 5) in a previous study [26]. The red triangles (n = 2) for a total 16 APL cases show the clinical APL samples whose microarray data were obtained in this study.
doi:10.1371/journal.pone.0111082.g003

(david.abcc.ncifcrf.gov/). In the induced APL cases, the genes related to N-Glycan, steroid and heparan sulfate biosynthesis, the spliceosome and pyrimidine metabolism were expressed similar to the levels in normal $CD34^+$ cells, and those related to the MAPK signaling pathway were exclusively expressed in comparison to normal myeloid cells, including normal $CD34^+$ cells. On the other hand, the genes related to neurotrophin signaling and the cell cycle, as well as those associated with metabolic processes, such as glycolysis/gluconeogenesis, the pentose phosphate pathway and sphingolipid metabolism were downregulated (**Table S2**), thus suggesting that the induced APL exhibited dysregulated signaling and metabolism as differentiated myeloid cells. Additionally, the gene set composed of 573 probes including 547 genes, which fulfilled one or more above criteria (ii) to (iv) in the gene set identified in (i), clearly separated the normal and malignant promyelocytes, such as those of induced and human primary APL (**Figure S5 and Table S3**), as described in the previous study using primary APL cases [26].

To evaluate the additional genetic events that accompanied the integration of *PML-RARA* in the genome, the insertion sites of *PML-RARA* were analyzed. Some of the integration sites of *PML-RARA* were in the introns or exons of genes (**Table S4**). However, they were neither recurrent nor found in the previous whole genome sequence analysis of the APL patients [33]. These findings suggest that *PML-RARA* was a common key event, but that there were various additional genetic events in these induced APL cells, and this finding was compatible with the previous analysis using human primary APL [33].

The induced APL cells differentiated into mature neutrophils following treatment with all-*trans* retinoic acid (ATRA) *in vitro* (**Figures 4A and 4B**), which was accompanied by alterations in the PML distribution in the nucleus, from a microspeckled to a speckled pattern (**Figure 4C**). Similarly, ATRA induced transient myeloid differentiation *in vivo* (n = 4), as has been seen in APL patients (**Figures 4D and 4E**).

These findings demonstrate that our induced APL cells recapitulate human APL both phenotypically and functionally.

## Re-transplantable cellular fraction in the induced APL cells

It is necessary to prove that the resultant induced APL cells possess the reproducibility of APL in the secondary recipients in order to demonstrate their capacity for leukemogenesis. However, previous studies have revealed that primary APL cells exhibit difficulty in engrafting in immunodeficient mice [3,12]. When the induced APL cells were transplanted into the second recipients, they were proven to be re-transplantable intravenously; 500,000 to 1,000,000 leukemic cells, but not 50,000 cells, were required, and the frequency of APL cells in the secondary recipients was low (0.04% to 1.41%, n = 6). The frequency was still low, even though

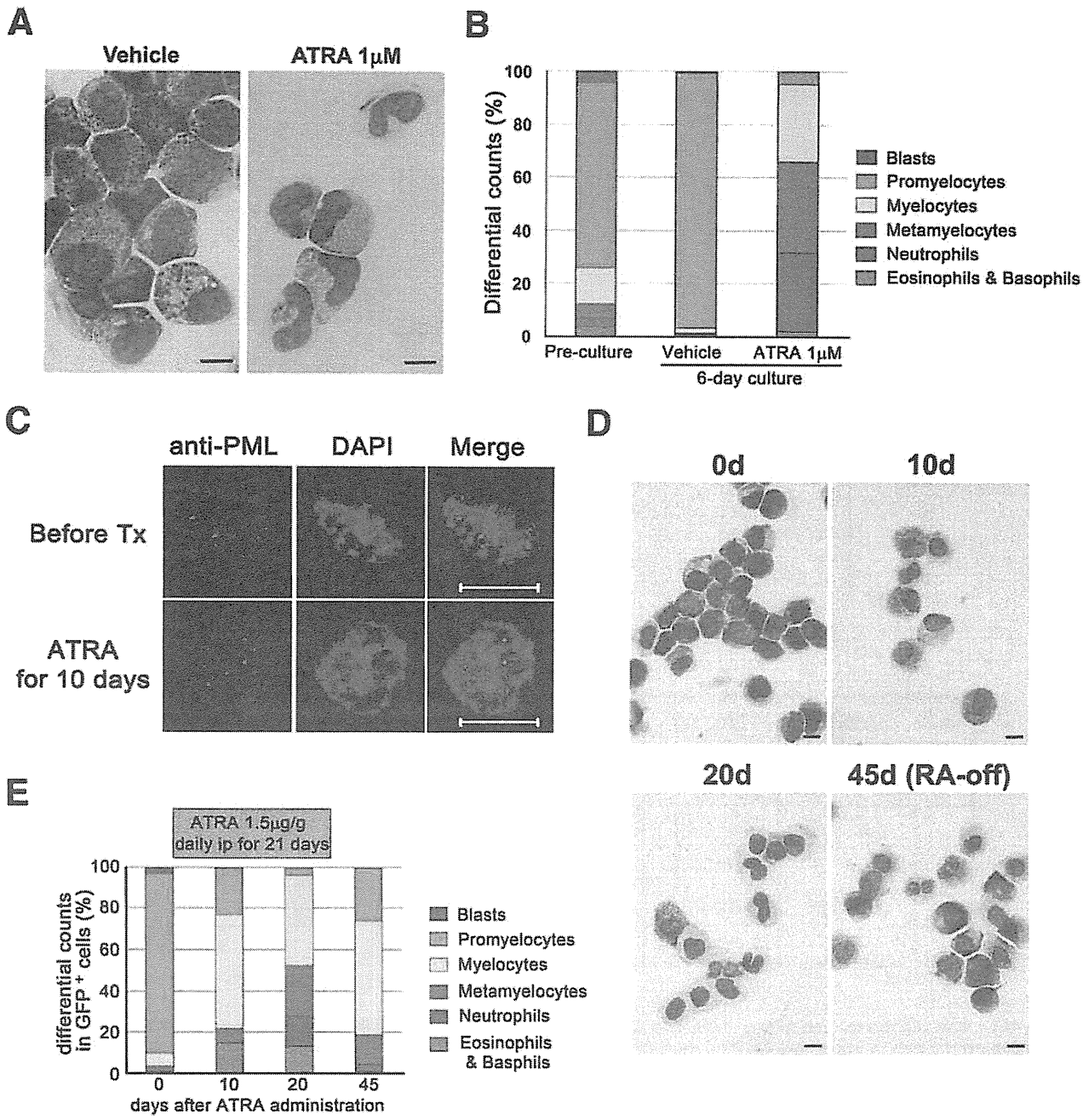


**Figure 4. The induction of myeloid differentiation in the APL cells induced by ATRA treatment *in vitro* and *in vivo*.** (**A**) Cytospin slides of the induced APL cells cultured with or without 1 μM ATRA for 6 days. The mature neutrophils with Auer rods are seen in the ATRA-treated group. The images were captured with a BX41 microscope (Olympus). The bar indicates 10 μm. (**B**) The differential cellular counts of the induced APL cells cultured with or without ATRA. The average leukocyte differentiation in three independent experiments is shown. (**C**) The results of an immunofluorescent analysis of the PML distribution in the induced APL cells before and after treatment with ATRA. The images were captured with an LSM510 META confocal microscope (Carl Zeiss). All the bars indicate 10 μm. (**D, E**) The induction of myeloid differentiation in the induced APL cells by ATRA *in vivo*. The secondary recipients transplanted with the induced APL cells were then intraperitoneally treated with ATRA for 21 days. Cytospin slides of $EGFP^+/hCD45^+/hCD33^+$ cells from the secondary recipients transplanted with the induced APL cells are shown (**D**). The images were captured with a BX41 microscope (Olympus). The bar indicates 10 μm. Their differentiated cellular counts were evaluated, and the representative series data are indicated (**E**).
doi:10.1371/journal.pone.0111082.g004

they were transplanted intramedullary (iBM, 2.00% to 5.98%, n = 2) (**Figure 5A**). The immunophenotype of the engrafted cells was the same as that seen in the primary induced APL cells: they were positive for CD13 and CD33, without the expression of CD34 or HLA-DR (**Figure 5B**), demonstrating that the induced APL retains self-renewal capacity with a low level of transplan-

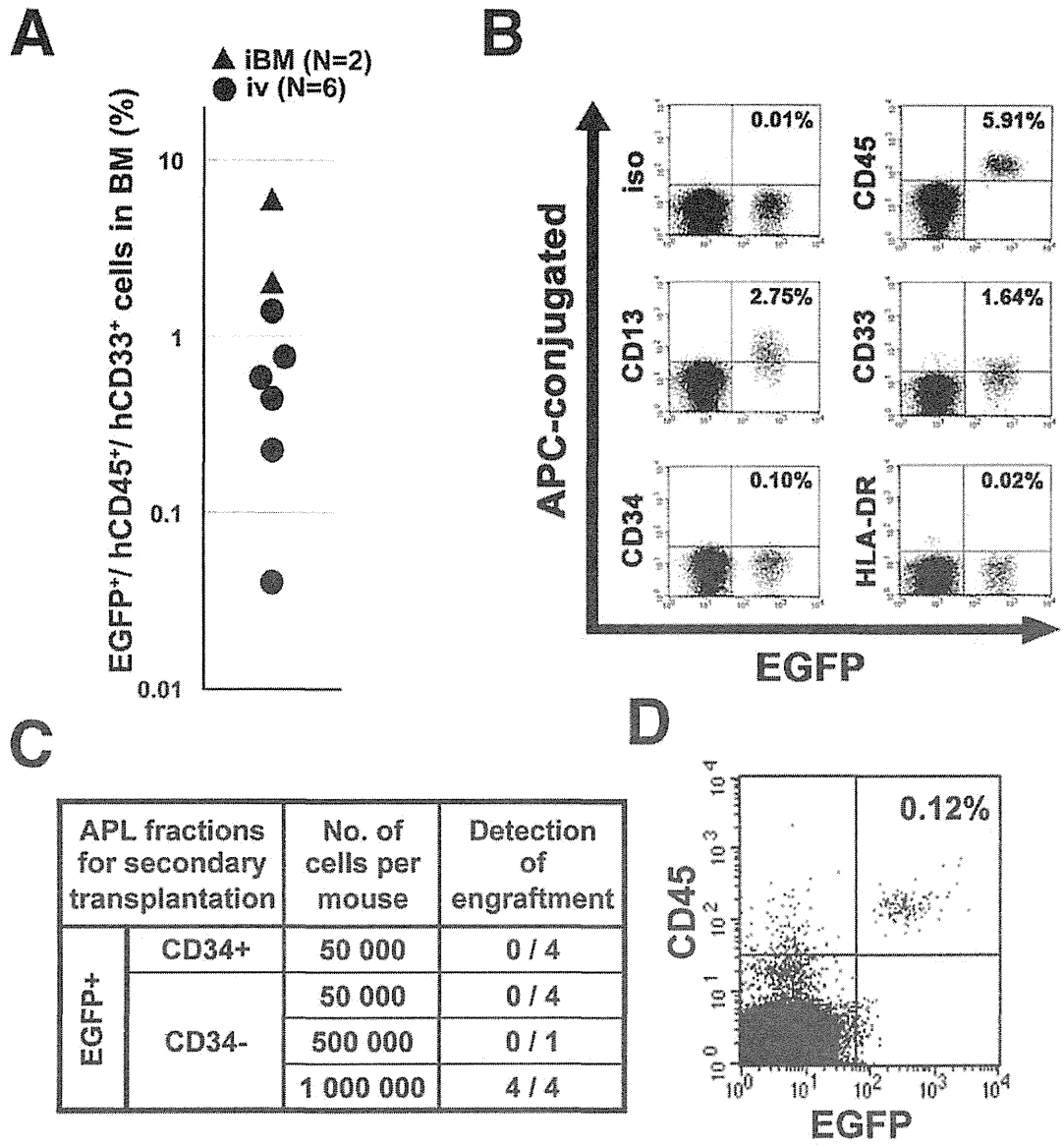


| APL fractions for secondary transplantation | | No. of cells per mouse | Detection of engraftment |
|---|---|---|---|
| EGFP+ | CD34+ | 50 000 | 0 / 4 |
| | CD34- | 50 000 | 0 / 4 |
| | | 500 000 | 0 / 1 |
| | | 1 000 000 | 4 / 4 |

**Figure 5. APL-LIC in the humanized APL *in vivo* model.** (A) The engraftment of the induced APL cells in the secondary recipients. The bone marrow cells were obtained 16 weeks after transplantation and evaluated. Each dot represents a single mouse. (B) The immunophenotype of the induced APL cells in the secondary recipients. The representative pattern is shown. (C) The engraftment capacity in each fraction from the induced APL cells in the secondary recipients. The bone marrow cells were obtained 16 weeks after transplantation and evaluated. (D) The engraftment of the $CD34^-$ fraction in the secondary recipients. The engrafted cells are shown as $EGFP^+/CD45^+$ cells.
doi:10.1371/journal.pone.0111082.g005

tation efficiency. In addition, the results suggested that the capacity for engraftment in this xenograft model differed between the $CD34^+$ cells transduced with *PML-RARA* and the APL cells mostly composed of the $CD34^-$ fraction.

To identify a fraction responsible for the APL maintenance in the induced APL cases, $CD34^+$ and $CD34^-$ APL fractions were separately collected and transplanted intravenously. The $CD34^+$ fraction was pooled because there were very few $CD34^+$ cells in each induced APL case (**Figures 3A and 5B**). The $CD34^-$ fraction was sorted twice to exclude the $CD34^+$ fraction completely. Fifty thousand APL cells in both the $CD34^+$ and $CD34^-$ fractions failed to engraft in the secondary recipients (0 out of 4 mice in each fraction). Similar to the unsorted cells, one million $CD34^-$ fraction cells were able to engraft in recipient mice (4 out of 4 mice) (**Figures 5C and 5D**).

These findings revealed that $CD34^-$ induced APL cells exhibit the ability to function as APL-LIC *in vivo*, although the LIC function was not excluded in the $CD34^+$ APL fraction.

## The $CD34^+/CD38^+$ progenitors trigger APL by *PML-RARA* induction *in vivo*

The findings that the *PML-RARA* transduced-$CD34^+$ cells developed APL while the resultant $CD34^-$ APL cells exhibited transplantability indicate the possibility that the initiation and maintenance of APL arise at different steps of differentiation, which are not likely to involve the $CD34^+/CD38^-$ fraction, as

originally reported in human AML. Therefore, in order to identify a cellular target for *PML-RARA* that effectively develops APL, *PML-RARA* was transduced into fractionated cells: $CD34^+/CD38^-$, $CD34^+/CD38^+$ and $CD34^-/CD33^+$ cells from the cord blood (**Figures 6A and 6B**). The transduction efficiency, as evaluated by EGFP expression, ranged from 1.9% to 5.0% (median: 3.53%, n = 6) in $CD34^+/CD38^-$ cells, 4.5% to 10.6% (median: 10.07%, n = 6) in $CD34^+/CD38^+$ cells and 19.1% to 22.1% (median: 20.63%, n = 4) in $CD34^-/CD33^+$ cells. Because the $CD34^+$ fraction from human cord blood possessed a higher proportion of $CD34^+/CD38^+$ (74.5% to 94.2%) than that of $CD34^+/CD38^-$ cells, the presumed absolute number of *PML-RARA* transplanted cells was higher in $CD34^+/CD38^+$ cells than in $CD34^+/CD38^-$ cells (3,430 to 31,800 cells vs 140 to 450 cells per mouse; 22,900 to 27,700 $CD34^-/CD33^+$ cells). One hundred unfractionated human $CD34^+$ cells, including both $CD34^+/CD38^-$ and $CD34^+/CD38^+$ cells, were engrafted with multilineage differentiation in our previous study [10], thus suggesting that the transplanted cell numbers were adequate for engraftment in the NOG mice. The induction of *PML-RARA* in $CD34^+/CD38^+$ cells reduced the colony formation capacity and favored the formation of myeloid colonies, as seen in $CD34^+$ cells (**Figures 1B and 1C**). On the other hand, the induction of *PML-RARA* in $CD34^+/CD38^-$ cells generated very few colonies in comparison to the MIGR1 control vector-infected $CD34^+/CD38^-$ cells (**Figures 6C and 6D**). Consistent with the results, the induced APL cells were detected mostly in the mice transplanted with $CD34^+/CD38^+$ cells (median, 16.4% in the whole bone marrow cells) (**Figure 6E**). These findings suggest that $CD34^+/CD38^+$ progenitors proliferate and survive more efficiently than $CD34^+/CD38^-$ cells *in vitro* and trigger APL *in vivo* by inducing *PML-RARA*.

### Human common myeloid progenitors develop into APL by inducing *PML-RARA* among $CD34^+/CD38^+$ progenitors

In order to identify the detailed target fraction in $CD34^+/CD38^+$ cells that generates APL with *PML-RARA*, the $CD34^+/CD38^+$ cells were then divided into three fractions based on their expression of CD123 and CD45RA; CMP, GMP and MEP (**Figure 6F**). The retroviral transduction efficiencies of *PML-RARA* into CMP, GMP and MEP were 6.0% to 15.2% (median: 6.6%, n = 9), 3.3% to 8.8% (median: 7.1%, n = 8), and 7.8% to 24.6% (median: 8.5%, n = 7) (**Figure 6G**), and the presumed absolute numbers of *PML-RARA* transduced cells in CMP, GMP and MEP utilized for the transplantation were 5,850 to 15,200, 830 to 4,250, and 1,150 to 2,550 cells per mouse, respectively, which were deduced to directly reflect their proportion in the human cord blood. The frequency of induced APL cells in whole bone marrow cells from transplanted NOG mice was higher when using CMP (median, 25.2%) than GMP and MEP (median, 0.15% and 0.01%, respectively) (**Figure 6H**).

Taken together, these findings obtained using our humanized *in vivo* APL model demonstrate that CMP are a target fraction for *PML-RARA* in the development of APL.

## Discussion

Our present study revealed that a humanized APL model was successfully established by transplantation of human $CD34^+$ cord blood transduced with *PML-RARA* into immunodeficient mice. Using this model, we demonstrated that the CMP develop into APL by transducing *PML-RARA* whereas the resultant $CD34^-$ APL cells had the ability to maintain the tumor. Our system improves in the following points: The induced APL cells were detected in all of the mice within 150 days if more than 3,000 human $CD34^+$ cells infected with *PML-RARA* were transplanted into NOG mice. The resultant leukemia well recapitulated the human disease phenotypically, genetically and functionally, including the presence of Auer rods and Faggot cells, and the expression pattern of cellular surface markers and transcripts, as well as ATRA sensitivity and low leukemia transplantability. These findings demonstrated that this humanized *in vivo* model is suitable for prospectively analyzing the process of APL development in humans.

The cellular subset from which the APL originates is still controversial. Several lines of evidence using *in vivo* experiments have suggested that APL arises in the committed myeloid progenitors, whereas several clinical observations using FISH and RT-PCR analyses suggest that APL arises in earlier progenitors [4]. A recent report using conditional knock-in mice showed that the induction of *PML-RARA* led to dominant proliferation in a stem cell compartment with multilineage potential, but did not result in myeloproliferation, as if the stem cell compartment would not support leukemogenesis in this model [34,35]. Our *in vitro* and *in vivo* findings are compatible with the previous findings which showed that the generation of *PML-RARA* transgenic mice was only possible by expressing *PML-RARA* in early myeloid cells using the human cathepsin G (hCG) and MRP8 promoters, not the promoters of β-actin, a housekeeping gene, and CD11b which is expressed at a later stage of myeloid differentiation [36].

The leukemogenic function of PML-RARα may require subtle myeloid differentiation, as seen in CMP in the present study; PML-RARα has been reported to possess the inhibitory or toxic effects on the cellular survival, senescence or apoptosis [18,37,38]. CMP are still immature enough to easily acquire stemness and are already committed to the myeloid lineage, which may allow *PML-RARA* to dysregulate RARα-dependent myelopoiesis, rather than hematopoietic stem cells, in agreement with the fact that *RARA* is implicated in the regulation of myelopoiesis, including both early stage and terminal differentiation. In this scenario, the expression of *PML-RARA* would induce differentiation of CMP to promyelocytes, but inhibit their terminal differentiation at the same time [19,39,40]. Therefore, if the CMP expressing *PML-RARA* acquires stemness, this can result in the development of APL. Our findings showed no engraftment of $CD34^+/CD38^-$ cells with *PML-RARA* transduction *in vivo*, although their leukemogenic activity cannot be denied, as fewer cells were transplanted in comparison to the $CD34^+/CD38^+$ cells. Further analyses are required to evaluate whether $CD34^+/CD38^-$ cells possess the ability to cause APL.

Xenograft models using immunodeficient mice are at present the only method for evaluating the maintenance of human leukemia as LIC. The induced APL generated in the NOG mice had a low engraftment efficiency; however, this biological feature well-reproduced the properties of APL cells found in human patients [3,12]. It is possible that the difficulty associated with engrafting APL cells, both primary samples and induced APL cells obtained from cord blood, into NOG mice may depend on the different preferences of human hematopoietic cells between humans and mice. The reconstitution of the human hematopoietic system in NOG mice is achieved with the dominant engraftment of B-cells, in comparison to the myeloid lineage cells [10]. This technical feature may affect the engraftment of each of the transplanted cellular subsets in our study. The slow progressive myeloid tumor cells, such as those involved in myelodysplastic syndromes and chronic myeloid leukemia in the chronic phase, were shown to be difficult to engraft in NOD/SCID-β2-

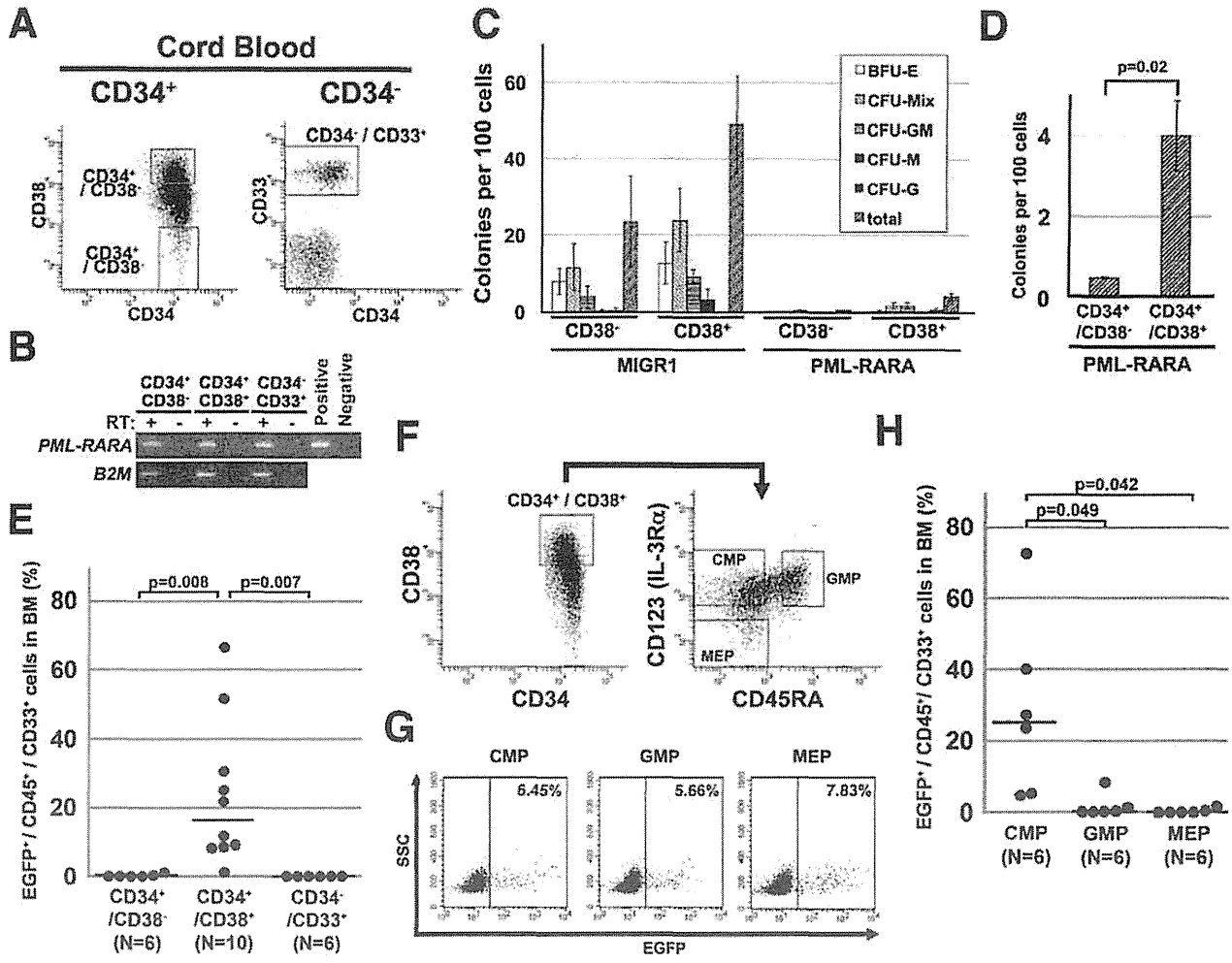


**Figure 6. *PML-RARA* targeted human common myeloid progenitors for APL leukemogenesis.** (**A**) The sorting strategy for $CD34^+/CD38^-$, $CD34^+/CD38^+$ and $CD34^-/CD33^+$ cells. Human cord blood was first separated into $CD34^+$ and $CD34^-$ cells by magnetic beads, and then sorted into three fractions by a FACS vantage instrument. (**B**) The expression of *PML-RARA* mRNA in each of the fractions after retroviral transfection. *B2M, beta 2 microglobulin*. The *PML-RARA* expression vector was used as a positive control for the *PML-RARA* analysis. (**C**) A colony-forming assay using *PML-RARA*-transduced $CD34^+/CD38^+$ and $CD34^+/CD38^-$ cells. The average of three independent experiments is shown. The data represent the means ± SD. (**D**) The total numbers of colonies of *PML-RARA*-transduced $CD34^+/CD38^+$ and $CD34^+/CD38^-$ cells shown in (C) are highlighted. The data represent the means ± SD (n = 3). (**E**) The development of the induced APL from $CD34^+/CD38^+$ cells in NOG mice. Each sorted fraction from human cord blood, as seen in (A), was retrovirally transduced with *PML-RARA* and transplanted into irradiated NOG mice. The percentages were determined by the frequency of $EGFP^+/CD45^+/CD33^+$ cells at 16 to 20 weeks after transplantation. Each dot represents a single mouse. The horizontal line represents the median value. (**F**) The sorting strategy for common myeloid progenitors (CMP), granulocyte-monocytic progenitors (GMP), and megakaryocyte-erythrocyte progenitors (MEP). Human cord blood was separated into $CD34^+$ cells by magnetic beads, $CD34^+/CD38^+$ cells were sorted out, and were finally divided into CMP, GMP and MEP by the FACS vantage instrument. (**G**) The transduction efficiency of *PML-RARA* in CMP, GMP and MEP. Representative data are shown. (**H**) The development of the induced APL from the human hematopoietic progenitors in NOG mice. Each sorted progenitor fraction from human cord blood, as seen in (F), was retrovirally transduced with *PML-RARA* and transplanted into irradiated NOG mice. The percentages were determined by the frequency of $EGFP^+/CD45^+/CD33^+$ cells at 16 to 20 weeks after transplantation. Each dot represents a single mouse. The horizontal line represents the median value.
doi:10.1371/journal.pone.0111082.g006

microglobulin-deficient or NOG mice (the previous reports [41–43] and our unpublished data), suggesting that the engraftment failure did not always indicate a lack of leukemogenecity of the transplanted cells. Therefore, our study confirmed the leukemogenic activity of the $CD34^-$ induced APL fraction, although it was not strong. These results are consistent with the previous *in vivo* reports which described the some primary $CD34^+/CD38^+$ and $CD34^-$ AML cells could function as LIC *in vivo* [44,45].

In conclusion, we demonstrated that the induction of *PML-RARA* targeted human $CD34^+$ cells, including CMP, and led to their ability to cause APL, and that $CD34^-$ APL cells have the capability of maintaining the disease. These findings suggest that it is not necessary that LIC are always consistent with a cellular fraction where leukemia-inducing events occur. Tumor-specific oncogenes, such as *PML-RARA*, effectively function to form tumors with specific characteristics in specific hierarchal stages of myelopoiesis. This model differs from the conventional hierarchal system of AML, in which LIC possess an immature phenotype as seen in hematopoietic stem cells. Since AML is a group of heterogeneous diseases with various causal genetic abnormalities,

the present findings will be helpful for the analysis of leukemogenesis in other types of AML which display differentiated leukemic blasts.

## Supporting Information

**Figure S1** The detection of *PML-RARA* expression in $CD34^+$ cells transduced with *PML-RARA* and their descendent colonies by qualitative RT-PCR. RT, reverse transcription.
(TIF)

**Figure S2** Fluorescent images of the colonies derived from the $EGFP^+$ and $EGFP^-$ fractions of the $CD34^+$ cells transduced with *PML-RARA*.
(TIF)

**Figure S3** The results of a quantitative analysis of the *PML-RARA* expression in the $CD34^+$ cells 48 hours after *PML-RARA* transduction, the differentiated cells from the resultant colonies and the induced APL cells. There were significant differences in the comparison of the expression level of *PML-RARA*. * indicates p values $<0.05$.
(TIF)

**Figure S4** The heat map of the microarray analysis using the 3,439 probes (3,278 genes) that were differentially expressed in the induced APL (n = 3) and the AML other than APL (n = 62). The gene set separated the induced and human primary APL from the cases of AML other than APL. Red triangles (n = 2 from the total of 16 APL cases) show the clinical APL samples whose microarray data were obtained in this study.
(TIF)

**Figure S5** The heat map of the microarray analysis performed using the gene set composed of 573 probes (547 genes), which were specifically expressed in the induced APL in comparison to cases of AML other than APL and normal promyelocytes. The gene set clearly clustered the malignant promyelocytes, such as the induced and human primary APL, apart from the normal promyelocytes. Red triangles (n = 2 of a total 16 APL cases) show the clinical APL samples whose microarray data were obtained in this study.
(TIF)

**Table S1** The sequences of the PCR primers and probes.
(XLSX)

**Table S2** KEGG pathway analysis with the gene sets aberrantly expressed in the induced APL.
(XLSX)

**Table S3** The gene set apllied in Figure S5 (573 probes).
(XLSX)

**Table S4** The integration sites of PML-RARA in the induced APL cells.
(XLSX)

## Acknowledgments

We thank Dr. Warren S. Pear (University of Pennsylvania) for providing the MIGR1 retroviral vector, Dr. Toshio Kitamura (The University of Tokyo) for providing the PLAT-gp packaging cells, Dr. Guilherme Santos (Beth Israel Deaconess Medical Center, Harvard Medical School) for his valuable suggestions and comments, and Tomoko Uno and Tomomi Takanashi (Tokai University School of Medicine) for their expert technical assistance.

## Author Contributions

Conceived and designed the experiments: H. Matsushita KA. Performed the experiments: H. Matsushita TY YS YN YM H. Matsuzawa TS AD H. Miyachi. Analyzed the data: H. Matsushita TY MT HH. Contributed reagents/materials/analysis tools: MO MI PPP. Wrote the paper: H. Matsushita TY KA.

## References

1. Lowenberg B (2008) Acute myeloid leukemia: the challenge of capturing disease variety. Hematology Am Soc Hematol Educ Program: 1–11.
2. Lapidot T, Sirard C, Vormoor J, Murdoch B, Hoang T, et al. (1994) A cell initiating human acute myeloid leukaemia after transplantation into SCID mice. Nature 367: 645–648.
3. Bonnet D, Dick JE (1997) Human acute myeloid leukemia is organized as a hierarchy that originates from a primitive hematopoietic cell. Nat Med 3: 730–737.
4. Grimwade D, Enver T (2004) Acute promyelocytic leukemia: where does it stem from? Leukemia 18: 375–384.
5. Hope KJ, Jin L, Dick JE (2004) Acute myeloid leukemia originates from a hierarchy of leukemic stem cell classes that differ in self-renewal capacity. Nat Immunol 5: 738–743.
6. Dick JE (2008) Stem cell concepts renew cancer research. Blood 112: 4793–4807.
7. Becker MW, Jordan CT (2011) Leukemia stem cells in 2010: current understanding and future directions. Blood Rev 25: 75–81.
8. de The H, Chen Z (2010) Acute promyelocytic leukaemia: novel insights into the mechanisms of cure. Nat Rev Cancer 10: 775–783.
9. Paietta E (2003) Expression of cell-surface antigens in acute promyelocytic leukaemia. Best Pract Res Clin Haematol 16: 369–385.
10. Ito M, Hiramatsu H, Kobayashi K, Suzue K, Kawahata M, et al. (2002) NOD/SCID/gamma(c)(null) mouse: an excellent recipient mouse model for engraftment of human cells. Blood 100: 3175–3182.
11. Yahata T, Ando K, Nakamura Y, Ueyama Y, Shimamura K, et al. (2002) Functional human T lymphocyte development from cord blood CD34+ cells in nonobese diabetic/Shi-scid, IL-2 receptor gamma null mice. J Immunol 169: 204–209.
12. Patel S, Zhang Y, Cassinat B, Zassadowski F, Ferre N, et al. (2012) Successful xenografts of AML3 samples in immunodeficient NOD/shi-SCID IL2R-gamma(-/-) mice. Leukemia 26: 2432–2435.
13. Guibal FC, Alberich-Jorda M, Hirai H, Ebralidze A, Levantini E, et al. (2009) Identification of a myeloid committed progenitor as the cancer-initiating cell in acute promyelocytic leukemia. Blood 114: 5415–5425.
14. Wojiski S, Guibal FC, Kindler T, Lee BH, Jesneck JL, et al. (2009) PML-RARalpha initiates leukemia by conferring properties of self-renewal to committed promyelocytic progenitors. Leukemia 23: 1462–1471.
15. Brown D, Kogan S, Lagasse E, Weissman I, Alcalay M, et al. (1997) A PMLRARalpha transgene initiates murine acute promyelocytic leukemia. Proc Natl Acad Sci U S A 94: 2551–2556.
16. Grisolano JL, Wesselschmidt RL, Pelicci PG, Ley TJ (1997) Altered myeloid development and acute leukemia in transgenic mice expressing PML-RAR alpha under control of cathepsin G regulatory sequences. Blood 89: 376–387.
17. He LZ, Tribioli C, Rivi R, Peruzzi D, Pelicci PG, et al. (1997) Acute leukemia with promyelocytic features in PML/RARalpha transgenic mice. Proc Natl Acad Sci U S A 94: 5302–5307.
18. Westervelt P, Lane AA, Pollock JL, Oldfather K, Holt MS, et al. (2003) High-penetrance mouse model of acute promyelocytic leukemia with very low levels of PML-RARalpha expression. Blood 102: 1857–1865.
19. Grignani F, Valtieri M, Gabbianelli M, Gelmetti V, Botta R, et al. (2000) PML/RAR alpha fusion protein expression in normal human hematopoietic progenitors dictates myeloid commitment and the promyelocytic phenotype. Blood 96: 1531–1537.
20. Manz MG, Miyamoto T, Akashi K, Weissman IL (2002) Prospective isolation of human clonogenic common myeloid progenitors. Proc Natl Acad Sci U S A 99: 11872–11877.
21. Pear WS, Miller JP, Xu L, Pui JC, Soffer B, et al. (1998) Efficient and rapid induction of a chronic myelogenous leukemia-like myeloproliferative disease in mice receiving P210 bcr/abl-transduced bone marrow. Blood 92: 3780–3792.
22. Matsushita H, Scaglioni PP, Bhaumik M, Rego EM, Cai LF, et al. (2006) In vivo analysis of the role of aberrant histone deacetylase recruitment and RAR alpha blockade in the pathogenesis of acute promyelocytic leukemia. J Exp Med 203: 821–828.
23. Kawada H, Ando K, Tsuji T, Shimakura Y, Nakamura Y, et al. (1999) Rapid ex vivo expansion of human umbilical cord hematopoietic progenitors using a novel culture system. Exp Hematol 27: 904–915.
24. Yahata T, Takanashi T, Muguruma Y, Ibrahim AA, Matsuzawa H, et al. (2011) Accumulation of oxidative DNA damage restricts the self-renewal capacity of human hematopoietic stem cells. Blood 118: 2941–2950.

25. Rego EM, He LZ, Warrell RP Jr, Wang ZG, Pandolfi PP (2000) Retinoic acid (RA) and As2O3 treatment in transgenic models of acute promyelocytic leukemia (APL) unravel the distinct nature of the leukemogenic process induced by the PML-RARalpha and PLZF-RARalpha oncoproteins. Proc Natl Acad Sci U S A 97: 10173–10178.
26. Payton JE, Grieselhuber NR, Chang LW, Murakami M, Geiss GK, et al. (2009) High throughput digital quantification of mRNA abundance in primary human acute myeloid leukemia samples. J Clin Invest 119: 1714–1726.
27. Ando K, Yahata T, Sato T, Miyatake H, Matsuzawa H, et al. (2006) Direct evidence for ex vivo expansion of human hematopoietic stem cells. Blood 107: 3371–3377.
28. Schmidt M, Hoffmann G, Wissler M, Lemke N, Mussig A, et al. (2001) Detection and direct genomic sequencing of multiple rare unknown flanking DNA in highly complex samples. Hum Gene Ther 12: 743–749.
29. Dyck JA, Maul GG, Miller WH Jr, Chen JD, Kakizuka A, et al. (1994) A novel macromolecular structure is a target of the promyelocyte-retinoic acid receptor oncoprotein. Cell 76: 333–343.
30. Weis K, Rambaud S, Lavau C, Jansen J, Carvalho T, et al. (1994) Retinoic acid regulates aberrant nuclear localization of PML-RAR alpha in acute promyelocytic leukemia cells. Cell 76: 345–356.
31. Grignani F, Testa U, Rogaia D, Ferrucci PF, Samoggia P, et al. (1996) Effects on differentiation by the promyelocytic leukemia PML/RARalpha protein depend on the fusion of the PML protein dimerization and RARalpha DNA binding domains. EMBO J 15: 4949–4958.
32. Paietta E, Goloubeva O, Neuberg D, Bennett JM, Gallagher R, et al. (2004) A surrogate marker profile for PML/RAR alpha expressing acute promyelocytic leukemia and the association of immunophenotypic markers with morphologic and molecular subtypes. Cytometry B Clin Cytom 59: 1–9.
33. Welch JS, Ley TJ, Link DC, Miller CA, Larson DE, et al. (2012) The origin and evolution of mutations in acute myeloid leukemia. Cell 150: 264–278.
34. Welch JS, Yuan W, Ley TJ (2011) PML-RARA can increase hematopoietic self-renewal without causing a myeloproliferative disease in mice. J Clin Invest 121: 1636–1645.
35. Wartman LD, Welch JS, Uy GL, Kleo JM, Lamprecht T, et al. (2012) Expression and function of PML-RARA in the hematopoietic progenitor cells of Ctsg-PML-RARA mice. PLoS One 7: e46529.
36. Puccetti E, Ruthardt M (2004) Acute promyelocytic leukemia: PML/RARalpha and the leukemic stem cell. Leukemia 18: 1169–1175.
37. Ferrucci PF, Grignani F, Pearson M, Fagioli M, Nicoletti I, et al. (1997) Cell death induction by the acute promyelocytic leukemia-specific PML/RARalpha fusion protein. Proc Natl Acad Sci U S A 94: 10901–10906.
38. Grignani F, Ferrucci PF, Testa U, Talamo G, Fagioli M, et al. (1993) The acute promyelocytic leukemia-specific PML-RAR alpha fusion protein inhibits differentiation and promotes survival of myeloid precursor cells. Cell 74: 423–431.
39. Collins SJ (2002) The role of retinoids and retinoic acid receptors in normal hematopoiesis. Leukemia 16: 1896–1905.
40. Du C, Redner RL, Cooke MP, Lavau C (1999) Overexpression of wild-type retinoic acid receptor alpha (RARalpha) recapitulates retinoic acid-sensitive transformation of primary myeloid progenitors by acute promyelocytic leukemia RARalpha-fusion genes. Blood 94: 793–802.
41. Thanopoulou E, Cashman J, Kakagianne T, Eaves A, Zoumbos N, et al. (2004) Engraftment of NOD/SCID-beta2 microglobulin null mice with multilineage neoplastic cells from patients with myelodysplastic syndrome. Blood 103: 4285–4293.
42. Kerbauy DM, Lesnikov V, Torok-Storb B, Bryant E, Deeg HJ (2004) Engraftment of distinct clonal MDS-derived hematopoietic precursors in NOD/SCID-beta2-microglobulin-deficient mice after intramedullary transplantation of hematopoietic and stromal cells. Blood 104: 2202–2203.
43. Muguruma Y, Matsushita H, Yahata T, Yumino S, Tanaka Y, et al. (2011) Establishment of a xenograft model of human myelodysplastic syndromes. Haematologica 96: 543–551.
44. Taussig DC, Vargaftig J, Miraki-Moud F, Griessinger E, Sharrock K, et al. (2010) Leukemia-initiating cells from some acute myeloid leukemia patients with mutated nucleophosmin reside in the CD34(-) fraction. Blood 115: 1976–1984.
45. Eppert K, Takenaka K, Lechman ER, Waldron L, Nilsson B, et al. (2011) Stem cell gene expression programs influence clinical outcome in human leukemia. Nat Med 17: 1086–1093.